

Modern Software Approaches For Fast Algorithms

Srinath Kailasa

A thesis submitted in partial fulfillment of the requirements
for the degree Doctor of Philosophy

Department of Mathematics
University College London
September, 2023

Declaration

I, Srinath Kailasa, confirm that the work presented in this thesis is my own. Where information has been derived from other sources, I confirm that this has been indicated in the thesis.

Abstract

Software has come to be a central asset produced during computational science research. Projects that build off the research software outputs of external groups rely on the software implementing proper engineering practice, with code that is well documented, well tested, and easily extensible. As a result research software produced in the course of scientific discovery has become an object of study itself, and successful scientific software projects that operate with performance across different software and hardware platforms, shared and/or distributed memory systems, can have a dramatic impact on the research ecosystem as a whole. Examples include projects such as the SciPy and NumPy projects in Python, OpenMPI for distributed memory computing, or the package manager and build system Spack, which collectively support a vast and diverse ecosystem of scientific research.

This thesis is concerned with the development of a software platform for so called ‘fast algorithms’. These algorithms have emerged in recent decades to optimally apply and invert dense matrices that exhibit a special low-rank structure in their off-diagonal elements. Such matrices arise in numerous areas of science and engineering, for example in the linear system matrices of boundary integral formulations of problems from acoustics and electromagnetics to fluid dynamics, geomechanics and even seismology. In the best case matrices can be stored, applied and inverted in $O(N)$, in contrast to $O(N^2)$ for storage and application, and $O(N^3)$ for inversion when computed naively. The diversity of the implementation approaches for these algorithms, as well as their mathematical intricacy, makes the development of an ergonomic, unified, software framework, that maximally re-uses data structures, is designed for high performance, distributed memory environments, and works seamlessly across platforms highly challenging. To date, many softwares for fast algorithms are often written to benchmark the power of a particular implementation approach, rather than with real user in mind.

Modern programming environments are diverse, with unique trade-offs, in Chapter 1 we document our experience in transitioning from Python to Rust as a modern, ergonomic, programming environment for our software. Chapter 2 introduces fast algorithms in the context of current work streams, specifically the implementation of a library for distributed memory octrees, and a distributed memory fast multipole method (FMM) built on top of this. Chapter 3 documents active areas of research and development for these projects, and proposed strategies for outstanding issues. We conclude by looking ahead at the requirements for the timely completion of this project as well as proposed extension areas.

Contents

1	Modern Programming Environments for Science	1
1.1	Developing Scientific Software	1
1.2	Pitfalls of Performant High Level Language Runtimes	2
1.3	Introducing Rust for Scientific Software	7
1.4	Emerging Developments	10
2	Designing Software for Fast Algorithms	12
2.1	The Fast Multipole Method	12
2.2	Algebraic FMM Variants	16
2.3	Implementation Challenges for the Kernel Independent Fast Multi- pole Method	20
2.4	Building for Re-Use in Fast Algorithm Software	24
3	Open Work Streams	30
3.1	Distributed Octrees	30
3.1.1	Exposing Parallelism in A Distributed Memory FMM	33
3.2	Fast Field Translations	37
3.2.1	SVD Field Translations	37
3.2.2	FFT Field Translations	40
4	Conclusion	48
A	Deriving Local Expansion Coefficients from the Analytical Multi- pole Expansion in \mathbb{R}^2 for the Laplace kernel	49
B	Hyksort	51
C	The Adaptive Fast Multipole Method Algorithm	54
D	Well Posedness of Dirichlet Boundary Value Problems For The Laplace Equation	56
E	Distributed Octrees	58
E.1	Useful Properties of Morton Encodings	58
E.2	Algorithms Required for Constructing Distributed Linear Octrees . . .	58
	Bibliography	62

Modern Programming Environments for Science

1.1 Developing Scientific Software

Scientific software development presents a unique set of challenges. Although development teams are frequently small, they are tasked with producing highly optimised code that must be deployed across a myriad of hardware and software platforms. Moreover, there is a pressing need for comprehensive documentation and rigorous testing to ensure reproducibility. Given that many of these softwares arise within doctoral programs or other short-term projects, there is a tendency to tailor software development to showcase a specific project’s objectives. Whether that be to demonstrate a convergence result of a specific methodological improvement, or offer a new benchmark implementation of an algorithm. Consequently, once the principal results are achieved these software projects often become orphaned, lack compatibility with a range of development platforms, or aren’t adaptable to related challenges and subsequent research by other teams.

A recent survey of 5000 software tools published in computational science papers featured in ACM publications found that repositories for computational science papers had a median active development span of a mere 15 days. Alarming, one third of these repositories had a life cycle of less than one day [17]. Implying that upon the publication of the affiliated paper, software typically gets abandoned or, at best, receives private maintenance. This trend underscores the challenge of dedicating sustained resources in an academic setting to software upkeep, even when such maintenance is vital for reproducibility. It may also hint at a deficiency in professional software engineering expertise among computational researchers whose principal expertise lies elsewhere.

Therefore, confronting the challenge of developing maintainable research software relies on the choice of programming environment. Developers need to have a frictionless system for testing, documenting, using existing open-source solutions and building extensions to their code. Software design has to be general enough to extend to new algorithmic developments, but also malleable enough for external developers and users to adapt software to new usecases as well as their own needs. Building software for diverse software environments and target architectures should also be painless as possible to encourage large-scale adoption. Additionally, domain scientists who are typically not experienced in low-level software development require interfaces to familiar high level languages, which must be easy to maintain for core-developers.

In the early stages of this research project we experimented with Python, a high-level interpreted language, that has become a de-facto standard in data-science and

numerical computing for a wide variety of domain scientists. Recent years have seen the development of tools that allow for the compilation of fast machine-code from Python, allowing for multi-threading, and the targeting of both CPU and GPU architectures [21]. This approach takes advantage of the LLVM compiler infrastructure for generating fast machine code from Python via the Numba library, and is similar to other approaches to creating fast compiled code from high-level languages such as Julia [4]. We built a prototypical single-node multithreaded implementation of a fast algorithm, the fast multipole method (FMM), in Python to test the efficacy of this approach. However, we found that for complex algorithms writing performant Numba code can be challenging, especially when performance relies on low-level management of memory [19]. We summarise this experience in section 1.2. We identified Rust, a modern low-level compiled language, as a promising programming environment for our software. Rust has a number of excellent features for scientific software development, most notably the introduction of a ‘borrow checker’, that enforces the validity of memory references at compile time preventing the existence of data races in compiled Rust code, as well as its runtime ‘Cargo’, which offers a centralised system for dependency management, compilation, documentation and testing of Rust code. We summarise Rust’s benefits, as well as notable constraints, in section 1.3. We conclude this chapter by noting that language and compiler development for scientific computing is an active area of research, in section 1.4 we contrast Rust with emerging programming environments for scientific software.

1.2 Pitfalls of Performant High Level Language Runtimes

The evolution of computational science has been marked by the introduction and adoption of high-level interpreted languages that are designed to be user friendly, and cross platform. Starting with Matlab in the 1970s, followed by Python in the 1990s, and more recently Julia in the 2010s. High-level languages have significantly impacted scientific computing, offering efficient implementations of algorithms and introducing optimised data structures via projects such as NumPy and SciPy, as well as ergonomic cross platform build systems. While these languages facilitate easier experimentation, achieving peak performance often necessitates manual memory management or explicit instruction set level programming to ensure vectorisation on a given hardware target. A natural question for us when deciding on a programming environment for this project was whether advancements in high-level languages were sufficient for the implementation of ‘fast algorithms’. If they proved to be sufficient our software would be free of the so called ‘two language’ problem, in which a user friendly interfaces in a high-level language provides a front-end for a compiled language implementation of more data-intensive operations. This problem plagues academic software development, as resulting software relies on a brittle low-level interface between the high-level front-end, and low-level back-ends for performance critical code sections.

Recent strategies to enhance the performance of high-level languages have involved refining compiler technology. These projects are advertised as tools that allow developers to use high-level languages for quick algorithm experimentation, while leaving it to the compiler to produce efficient machine code. Benchmarks are usually offered with respect certain numerical operations that can be vectorized, such as iteration over aligned data structures, with compilers taking care to unroll

loops and apply inlining to inner function calls.

Noteworthy examples are the Numba project for Python and the Julia language. Both leverage the LLVM compiler infrastructure, which aims to standardize the back-end generation of machine code across various platforms. This approach, known as ‘just in time’ or JIT compilation, generates code at runtime from the types of a function’s signature. Figure 1.1 provides a sketch of how Numba in particular generates machine code from high-level Python code. The LLVM compiler supports numerous hardware and software targets, including platforms like Intel and Arm, and provides multithreading through support for compiler extensions such as OpenMP. Additionally, these compilers offer native support for GPU code generation. An important difference between Numba and Julia is that Numba is simply a compiler built to optimise code written for the numerical types created using the NumPy library, and Julia is a fully fledged language. Numba contains implementations of algorithms a subset of the scientific Python ecosystem, specifically functionality from the NumPy project for array manipulation and linear algebra.

As many performance benchmarks for these programming environments are typically provided for algorithms that rely on simpler data structures, we decided to test these high-level environments for more complex algorithms before making a choice about our programming environment for this project. We implemented a single node multi-threaded FMM using Python’s Numba compiler, identifying two notable pitfalls with this approach, the full results of which were recently published in *Computing in Science and Engineering* [19].

Firstly, JIT compilation of code imposes a significant runtime cost that is disruptive to development. Compiled functions are by default not cached between interpreter sessions in either Julia or Numba code. Our FMM code takes 15 ± 1 s to compile when targeting a i7-9750H CPU with x86 architecture, where the benchmark is given with respect to seven runs. This is comparable to the runtime of the FMM software for a typical benchmark FMM problem ¹. For smaller problem sizes, the compilation time dominates runtime. Ahead of time (AOT) compilation is partially supported in Numba, and can be used to build binaries for distribution to different hardware targets, e.g. x86 or ARM. However support for AOT compiled code is currently second class, the machine code created in this manner are usable only from the Python interpreter and not from within calls made from other Numba compiled functions, and it’s currently staged for deprecation and replacement. We note that Julia does support AOT compilation via the `PackageCompiler.jl` module. This allows for different levels of AOT compilation, from creating a ‘sysimage’ which amounts to a serialised file containing the compiled outputs of a Julia session, a relocatable ‘app’ which includes an executable compiled to a specific hardware target alongside Julia itself, to creating a C library which can be precompiled for a specific hardware target such as x86. However, this requires relatively advanced software engineering skills, and raises the barrier to entry for high-performance computing with Julia.

Thus switching to such a programming environment requires developers to create a workflow that keeps interpreter sessions active for as long as possible in order to reduce the impact of long compilation times, or write build scripts for AOT compilation for a specific hardware target similar to compiled languages. As one of the key advantages of high-level languages is their developer friendliness and simple

¹1e6 particles distributed randomly, using order $p = 6$ expansions for a Laplace problem takes approximately 30s on this hardware using our software. See Chapter 2 for more details on the FMM and the significance of these terms.

build systems this acts as an impediment.

Downstream users of software, who may also be using JIT compilers for their own code, are faced with significant compilation times, and potentially intricate build steps unless catered for by the original library’s developers. This problem compounds in the case of distributed memory programs using MPI, as JIT compilation imposes runtime costs to the entire program. Unless a project has been distributed as a binary, by default MPI runs are not interactive, and therefore require a recompilation for each run. This isn’t to say MPI programs written in Julia or Numba haven’t been scaled to large HPC systems, however their usage does carry a cost in terms of developer workflow, and potentially program runtime.

Secondly, our experience in developing the FMM in Numba made clear how difficult it can be to anticipate the behaviour of Numba when considering how to optimise functions with different implementations of the same logic. Consider the code in Listing 1.1, here we show three logically equivalent ways of performing two matrix-matrix products, and storing a column from the result in a dictionary. A dictionary is chosen for storage as this mirrors the data structure used in our FMM software for storing intermediate results. The runtimes of all three implementations are shown in Table 1.1 for different problem sizes. We choose this example because this operation of matrix-matrix multiplication is well supported by Numba, and data instantiation, whether from within or external to a Numba compiled function, should in principle make little difference as the Numba runtime simply dereferences pointers to heap allocated memory when entering a Numba compiled code segment. This example is designed to illustrate how arbitrary changes to writing style can impact the behavior of Numba code. The behavior is likely due to the initialisation of a dictionary from within a calling Numba function, rather than an external dictionary, and having to return this to the user. However, the optimisations taken by Numba are presented opaquely to a user and it’s unclear why there are performance variations at all.

In developing our FMM code we faced significant challenges in tweaking our code and data structures to maximise the performance achieved from within Numba. From manually inlining subroutines as in Listing 1.1, to testing where to allocate data. Our final code took a significant amount of time to develop, approximately six months, and was organised in a manner that optimised for performance rather than readability. Thus, despite being a *compiler* for numerical Python, Numba behaved in practice more like a *programming framework* which a developer had to adhere to strictly in order to achieve the highest-level of performance. The disadvantage of this is that the framework is both relatively restrictive, but also presented opaquely to a user.

Therefore, while being an amazing technology with great features, Numba was not decided to be a suitable choice for our programming environment. Its ability to target a diverse set of hardware targets from Python, leveraging the power of LLVM to write multithreaded, and autovectorised code, as well as writing CPU and GPU code from within Python, while allowing downstream projects to develop in a familiar language with a large open-source ecosystem and simple dependency management demonstrate the utility of this remarkable tool. However, the constraints of high level languages, specifically the inability to manage memory at a system level, as well as the development costs of JIT compilation, and Numba’s framework-like behaviour demonstrate that while being useful, it is preferable to write our software platform using a systems-level language where high-performance can be assumed. Our criticisms of Numba also apply to Julia. However we note that Julia has certain

advantages over Numba including its design and syntax focussed on mathematical computing, native support for multithreading, a richer type system and a large open-source community with a scientific computing focus.

System level languages have progressed commensurately to high-level languages over recent decades. Modern languages such as Go and Rust, offer runtimes with informative compilers, inbuilt documentation and testing facilities, as well as LLVM backends to support code generation across platforms, removing much of the complexity associated with building and distributing software written in C/C++. Rust in particular, uninhibited by a garbage collector as for Go, makes it easy to inter-operate Rust code with libraries built in C/C++ via its foreign function interface, making it simple to leverage existing open-source scientific software. We therefore conclude that the two language problem is minimised in comparison to the past, and modern system level programming languages potentially offer an effective solution for building academic software.

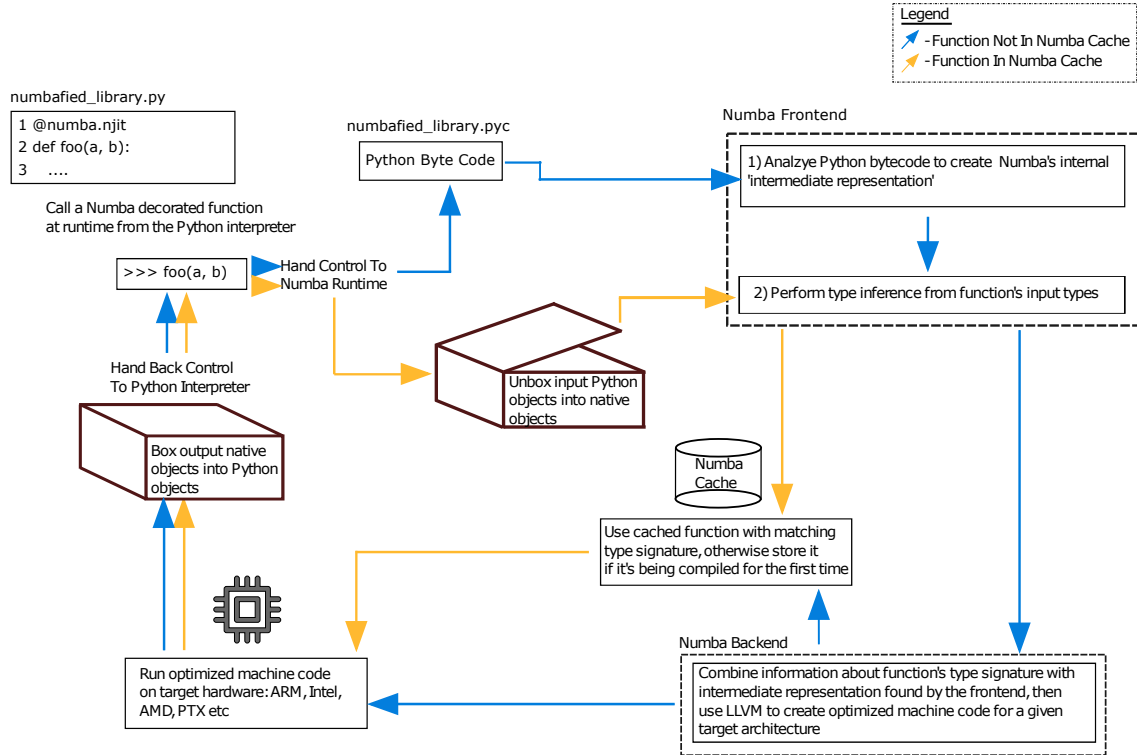


Figure 1.1: A visualisation of the Numba runtime system. A function decorated with ‘njit’ acts as an instruction to the runtime to check a database for any Numba-compiled functions with a matching function signature, if this doesn’t exist Numba generates a new compiled function and caches it using LLVM. Future calls of this function use this cached version in place of the Python interpreter. Code relies on Numba’s runtime to correctly ‘box’ and ‘unbox’ native Python objects into data structures compatible with Numba code, which operates on a subset of numerical data structures created using the NumPy library. Figure adapted from [19].

```
1 import numpy as np
2 import numba
3 import numba.core
4 import numba.typed
5
6 # Initialise in the Python interpreter
7 data = numba.typed.Dict.empty(
8     key_type=numba.core.types.unicode_type,
9     value_type=numba.core.types.float64[:]
10 )
11
12 data['initial'] = np.ones(N)
13
14 # Subroutine 1
15 @numba.njit
16 def step_1(data):
17     """
18     Initialise a matrix and perform a matrix matrix product,
19     storing a single column in the data dictionary.
20     """
21     a = np.random.rand(N, N)
22     data['a'] = (a @ a)[0,:]
23
24
25 # Subroutine 2
26 @numba.njit
27 def step_2(data):
28     """
29     Initialise a matrix and perform a matrix matrix product,
30     storing a single column in the data dictionary.
31     """
32     b = np.random.rand(N, N)
33     data['b'] = (b @ b)[0,:]
34
35
36 @numba.njit
37 def algorithm_1(data):
38     """
39     First implementation.
40     """
41     step_1(data)
42     step_2(data)
43
44
45 @numba.njit
46 def algorithm_2(data):
47     """
48     Second implementation.
49     """
50     # This time the storage dictionary is created within the
51     # Numba function, so the types are inferred by the Numba
52     # runtime, this also avoids a boxing cost to create a
53     Numba
```

```

53     # type from a Python one.
54     data = dict()
55     data['initial'] = np.ones(N)
56     step_1(data)
57     step_2(data)
58     return data
59
60 @numba.njit
61 def algorithm_3(data):
62     """
63     Third implementation.
64     """
65
66     # This time, the subroutines are manually inlined
67     # by the implementer, as well as the initialisation
68     # of the results dictionary locally, as in algorithm_2.
69
70     data = dict()
71     data['initial'] = np.ones(N)
72
73     def step_1(data):
74         a = np.random.rand(N, N)
75         data['a'] = (a @ a)[0,:]
76
77
78     # Subroutine 2
79     @numba.njit
80     def step_2(data):
81         b = np.random.rand(N, N)
82         data['b'] = (b @ b)[0,:]
83
84     step_1(data)
85     step_2(data)
86     return data

```

Listing 1.1: Three ways of writing a trivial algorithm in Numba, that performs some computation and saves the results to a dictionary. Adapted from Listing 2 in [19]

1.3 Introducing Rust for Scientific Software

Rust is a modern system-level programming language, introduced by Mozilla in 2015 as a direct replacement for C/C++, and is bundled with features that favour safety for shared memory programming. Having identified it as a suitable candidate for our programming environment, we list a few of its key benefits in this section.

Fortran and C/C++ have continued to dominate high-performance scientific computing applications, the main criticism of these languages for academic software is their relatively poor developer experience. C/C++ especially has significant flexibility in the compilers, documentation, build systems and package managers that developers can choose to work with, as well as support for multiple paradigms and a growing syntax. Rust stands in contrast to this with a single centrally supported runtime system, Cargo, with common standards for testing and documentation. Additionally, there is only a single Rust compiler, `rustc`. This inflexibility, in

Table 1.1: Performance of different algorithms from Listing 1.1, taken on an i7 CPU and averaged over seven runs for statistics.

Algorithm	Matrix dimension	Time (μs)
1	$\mathbb{R}^{1 \times 1}$	1.55 ± 0.01
1	$\mathbb{R}^{100 \times 100}$	304 ± 3
1	$\mathbb{R}^{1000 \times 1000}$	$29,100 \pm 234$
1	$\mathbb{R}^{1 \times 1}$	2.73 ± 0.01
1	$\mathbb{R}^{100 \times 100}$	312 ± 3
1	$\mathbb{R}^{1000 \times 1000}$	$25,700 \pm 92$
1	$\mathbb{R}^{1 \times 1}$	2.71 ± 0.01
1	$\mathbb{R}^{100 \times 100}$	312 ± 1
1	$\mathbb{R}^{1000 \times 1000}$	$25,700 \pm 140$

addition to a strongly preferred way of organising Rust code via its Traits system, makes Rust libraries significantly more uniform and readable than corresponding C++ code. Indeed installing a Rust library, or building a binary, is often as simple as running a single command from a terminal, or adding a single line to a TOML dependency file.

The lack of a uniform building and packaging standards in C/C++ means that some projects go as far as to implement a custom build system, such as the Boost library [2]. With the exception of Fortran, which has made recent strides to develop a standardised modern package manager and build system, inspired by Rust’s Cargo [13], C and C++ do not have a single officially supported package manager or build system. The resulting landscape is a multitude of package managers [33, 41, 11] and build systems [38, 3, 31] a few of which we have cited here, all of which replicate each others functionality, none of which are universally accepted or implemented across projects nor officially supported by the C++ software foundation. Figure (1.2) provides an overview of a few of the myriad approaches taken in other languages. To manage this complexity, builds are often defined using a metabuild system, most commonly CMake. CMake is a scripting language, and as a meta build system it takes a specification of local and third party dependencies and hardware targets, and generates Makefiles. CMake gives developers a great deal of flexibility, it is multi-platform, and language agnostic, however using it directly is not straightforward to maintain projects as dependencies grow, and to keep on top of dependency versions. Indeed, there is a significant body of literature discussing best practices with CMake [32]. However, CMake is not responsible for downloading and installing third party packages or verifying their relative compatibility, implementing its best practices is again left to users. Cargo’s relative simplicity mirrors the simple build systems of high-level languages such as Python or Julia, and removes one of the main causes of development pain when working with compiled languages, and makes it significantly easier for small teams to publish software that can be easily deployed by downstream users regardless of their system’s architecture or operating system.

A unique feature of Rust is its approach to ensure safe shared memory programming, enforced by its compile time ‘borrow checker’. Every reference in Rust has an associated ‘lifetime’ defined by its scope, and a singular ‘owner’. Which enforce the programming pattern of ‘resource allocation is initialisation’ (RAII). The basic rule is that references are owned within a scope, and dropped when out of scope. The

borrow checker enforces this at compile-time, in a multithreaded context this makes it impossible to have a compiled Rust binary that has dangling pointers or double-free errors. For mutable data, the borrow checker ensures that there is only a single mutable reference at any given time in the program's runtime, ensuring that there can never be a race condition in compiled Rust code. Identifying pointer-related bugs is one of the main challenges in multi-threaded programming, with safe 'smart pointers' being optional in C++, implementing RAII is left to developers.

Rust is 'multi-paradigm', supporting both object oriented, and functional styles of programming. Method calls are often chained, in a functional-like style, however users can still implement methods on structs as in other object oriented languages. The unique feature introduced by Rust is its Traits system, for specifying shared behaviour, that supersedes object-oriented design. Traits are similar to C++ 21's interfaces, in that they provide a way to enforce behaviour, rather than embedding it into a type as with traditional inheritance. However unlike C++, Rust Traits allow you to write blanket implementations, and implement interfaces for types you didn't define in your own code making them significantly more powerful. This means that behaviour can be built 'bottom up', rather than 'top down' as with object orientation, making it much easier for readers to identify the expected behaviour of a given Rust type by simply reading which Traits it implements. In a scientific context we are usually concerned with the organisation, reading and writing of data, commonly adhering to a design philosophy known to as data-oriented design. Traits allow us to inject additional behaviour on types without having to worry about potentially complex inheritance hierarchies.

Rust's runtime includes a test runner, a documentation generator, and a code formatter. As with other Rust features, these are maintained in lock step with the language specification, and with reference to other Rust developments. This imposes universal constraints on all Rust projects, allowing for objectively defined 'good' Rust code, rather than relying on various standards of best practices that vary between projects and organisations. Furthermore the Rust compiler is highly informative, providing hints to developers on best practices for their code, as well as potential sources of bugs or code rot, by notifying users of common anti-patterns or unused variables and functions.

Despite being a young language, Rust already supports a mature ecosystem of libraries for scientific computing with high-level multithreading support [35], numerical data containers [29], and tools for generating interfaces to Python via its C ABI [26]. Many tools are yet to be ported into native Rust, however high quality bindings exist for core tools such as MPI [34], BLAS and LAPACK [5], with simplified build steps often requiring only a few extra lines in the dependency TOML file. The problem with interfacing with tools written in other languages is also present when building software in Rust, however Cargo offers tools to build software written in other languages and integrate it with Rust code via the 'build.rs' package, which allows one to leverage existing build systems written for software written in foreign languages. This detracts from the benefits offered by Cargo as a unified package manager and build system, raising similar problems to those encountered when building software in other compiled languages. However, we observe that this remains a concern of the software's developer, who is responsible for providing build scripts for the operating systems and hardware platforms that they wish to support, and from a downstream user perspective their build process remains the same as with pure Rust packages, where the dependency is defined in their dependency TOML file. We also note that Rust is missing key tools for scientific computing,

such as a code generation for GPUs, however with mounting interest in Rust from the scientific computing community this is an active area of development.

1.4 Emerging Developments

Despite the above criticisms, high-level languages as tools for high-performance scientific computing remain an intense area of research and development. ‘Mojo’ is a new programming language, along with a compiler. It’s built as a superset of Python, specifically with the two-language problem in mind. Additionally, it attempts to address the ‘three language problem’, whereby languages also target exotic hardware such as GPUs and TPUs [23].

Led by a team that includes the original developers of LLVM, Mojo aims to simplify the development of high-performance applications in a Python-like language, that acts as a superset of Python. Moreover, it seeks to make these applications deployable across most hardware and software targets, ensuring compatibility with Python’s vast open-source libraries and straightforward build tools.

This is achieved by building on the MLIR compiler infrastructure. MLIR can be thought of as a generalisation of LLVM, catering to CPUs, GPUs, and novel ASICs for AI. The team chose to develop around Python to leverage its extensive existing user base in computational and data sciences.

Currently, Mojo remains a closed-source language and is actively being developed by its parent company, Modular. Thus, even though it appears promising, it’s not yet in a state suitable for experimentation. Nevertheless, Mojo showcases the potential of a future programming environment that might definitively ‘solve’ the problems developers face when selecting a programming environment for academic software.

Installing and Building Software in C++/Fortran

Builds for open source software are often **Readme Driven**. In this common approach developers provide a set of instructions for how to install a project's dependencies and the project itself. Common approaches include:

Dependency Management Methods



1) Simply add all dependencies to source tree of your project. Projects with a large number of dependencies can grow to have millions of lines of code, which can have a drastic effect on compilation times. Large C++ projects for example can take between several minutes to several hours to compile from source



2) Use a system package manager, and source from repositories such as GitHub to install globally. These can then be found by build systems. This makes it difficult to build isolated build environments, and configure builds with different versions, or sets, of dependencies.

Build Methods



1) Developer provided Make and Autotools scripts. lowest barrier to entry but build system will use globally installed dependency libraries, unless alternative provided. Makes multi-platform builds, or those using different software versions challenging.

2) Developer provided CMake scripts, to generate build systems for different environments. Again, reliant on globally installed dependency libraries.



Neither of these methods can check for dependency conflicts, which is left up to the developer to resolve.

Modern Package Management

Modern package managers allow for maximum safety and flexibility. They support multiple operating systems, compilers, build systems, and hardware microarchitectures, and are usually defined by recipes written in a simple scripting language such as Python, and can be used to generate build system scripts such as Makefiles and CMake scripts. They also support dependency tree checking for conflicting requirements, leading to stable builds. Two popular leading tools for HPC in C++ and Fortran are **Spack** and **Conan**.



Spack

- + Supported on Linux and MacOS.
- + Package recipes specified with Python scripts.
- + Over 5000 commonly used packages available.
- + Supports isolated environments, supporting building packages with from specific constraints, and clean global environment.
- + Can target hardware microarchitectures.
- + Growing support for binary package installation, though not available on all hardware targets.
- + Compatible with all major build systems, such as CMake and SCons
- No Windows support.



Conan

- + Supported on Linux, MacOS and Windows
- + Package recipes specified with Python scripts.
- + Supports isolated environments, supporting building packages with from specific constraints, and clean global environment.
- + Support for binary packages, speeding up installation times.
- + Compatible with all major build systems, such as CMake and SCons.

However, we note that even in 2021 modern package managers are still only used in a tiny fraction of all projects. For example Conan, only accounts for 5% of all C++ projects surveyed by JetBrains¹ in comparison to 21% of projects still relying on the system package manager, 26% simply including a dependencies source code as a part of a project's source tree, 23% using the readme driven build of each specific dependency, and 21% installing non-optimised precompiled binaries from the internet. Indeed only a small minority, 22%, used a package manager of any kind, with no solution taking a majority of even this market share. This is in stark contrast to the uniformity of the situation in Rust, in which all projects use Cargo as a build system and package manager and rustc as a compiler.

1. <https://www.jetbrains.com/lp/devecosystem-2021/cpp/>

Figure 1.2: An overview of building software in other compiled languages.

Designing Software for Fast Algorithms

2.1 The Fast Multipole Method

In this section we introduce the Fast Multipole Method (FMM), a foundational fast algorithm, the implementation of which is central to our software infrastructure. We begin by describing the FMM, first introduced by Greengard and Rokhlin in the 1980s, in the context of the solution of the N -body potential calculation problem of electrostatics, or gravitation, which gives rise to much of the terminology in this field [14]. We proceed to describe more modern algorithmic approaches, which retain many of the core algorithmic features of the original FMM while being more amenable to software implementation on modern computer hardware [24, 12]. We note that the FMM in its most basic form corresponds to a matrix-vector product, and we therefore conclude by briefly contrasting the FMM with similar methods for computing this quantity, as well as noting methods for computing the approximate inverse of FMM matrices, which correspond to a form of direct solver, termed ‘fast direct solvers’.

Consider the following N -body problem which appears in the calculation of electrostatic, or gravitational potentials from a set of point charges, or masses,

$$\phi_j = \sum_{i=1}^N K(x_i, x_j) q_i \quad (2.1)$$

Here, q_i is a point charge/mass, corresponding to N particles at positions x_i and the ‘kernel’ is defined as,

$$K(x, y) = \begin{cases} \log \|x - y\| & \text{in } \mathbb{R}^2 \\ \frac{1}{4\pi \|x - y\|} & \text{in } \mathbb{R}^3 \end{cases} \quad (2.2)$$

Writing the component form (2.2) as its corresponding linear system,

$$\phi = K \mathbf{q} \quad (2.3)$$

We note that the matrix K is *dense*, with non-zero off diagonal elements, and that this implies a global data dependency between all point charges/masses. This global data dependency had previously inhibited numerical methods for N -body problems as a naive application of this matrix requires $O(N^2)$ flops, and an finding an inverse using a linear algebra technique such as LU decomposition or Gaussian

Elimination requires $O(N^3)$ flops. The key insight behind the FMM, and subsequent fast algorithms, was that the interactions between physically distant groups of points could be compressed with a bounded accuracy if the kernel function exhibits amenable properties, specifically if it rapidly decays as the distance between two point sets increases. We demonstrate this in figure 2.1.

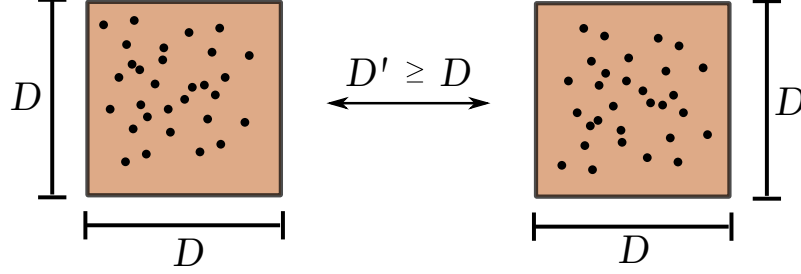


Figure 2.1: Given two boxes in \mathbb{R}^d ($d = 2$ or 3), \mathcal{B}_1 and \mathcal{B}_2 , which each enclose a corresponding set of points. The off-diagonal blocks in the matrix $K_{\mathcal{B}_1\mathcal{B}_2}$ and $K_{\mathcal{B}_2\mathcal{B}_1}$ are considered low rank and amenable to compression for the FMM when the distance separating them is at least equal to their diameter.

From figure 2.1 we see that the FMM relies on a discretisation that allows us to systematically compress far-interactions. To see how we obtain this, we start by placing our problem in a square/cube domain containing all N points, denoting this with Ω . Returning to (2.3), we must calculate the potential vector $\phi \in \mathbb{R}^N$, from a charge/mass vector $\mathbf{q} \in \mathbb{R}^N$ by applying $K \in \mathbb{R}^{N \times N}$. We begin with the situation in figure 2.1, where we have two sets of particles contained in boxes separated by some distance that makes their interaction amenable to compression, the FMM literature often describes such boxes as being ‘well separated’. Labelling the boxes as Ω_s and Ω_t , containing ‘source’ particles $\{y_j\}_{j=1}^M$, with associated charges/masses q_j , and ‘target’ particles $\{x_i\}_{i=1}^N$ respectively, we seek to evaluate the potential introduced by the source particles at the target particles. As the interaction assumed to be amenable to compression we are able to write an approximation to (2.1) using a low-rank approximation for the kernel in terms of tensor products as,

$$K(x, y) \approx \sum_{p=0}^{P-1} B_p(x) C_p(y), \quad \text{when } x \in \Omega_t, y \in \Omega_s \quad (2.4)$$

Where P is called the ‘expansion order’, or ‘interaction rank’. This is equivalent to approximating the kernel with an SVD using its leading singular values. We introduce index sets I_s and I_t which label the points inside Ω_s and Ω_t respectively, and find a generic approximation for the charges/masses,

$$\hat{q}_p = \sum_{j \in I_s} C_p(x_j) q_j, \quad p = 0, 1, 2, \dots, P-1 \quad (2.5)$$

Using this we can evaluate an approximation to the potential due to these particles in the far-field as,

$$\phi_i \approx \sum_{p=1}^{P-1} B_p(x_i) \hat{q}_p \quad (2.6)$$

In doing so we accelerate (2.1) from $O(MN)$ to $O(P(M + N))$. As long as we choose $P \ll M$ and $P \ll N$, we recover an accelerated matrix vector product for calculating the potential interactions between the set of sources and targets from two well separated boxes. The rapid decay behaviour of the kernel ensures that we can recover the potential in Ω_t with high-accuracy even if P is small. We note that although we represent the sources/targets as corresponding to different particle sets in this derivation they may be equivalent.

We deliberately haven't stated how we calculate B_p or C_p . In Greengard and Rokhlin's original FMM these took the form of analytical multipole and local expansions of the kernel function [14]. To demonstrate this we derive an expansion in the \mathbb{R}^2 case, taking c_s and c_t as the centres of Ω_s and Ω_t respectively,

$$\begin{aligned} K(x, y) &= \log(x - y) = \log((x - c_s) - (y - c_s)) \\ &= \log(x - c_s) + \log\left(1 - \frac{y - c_s}{x - c_s}\right) \\ &= \log(x - c_s) - \sum_{p=1}^{\infty} \frac{1}{p} \frac{(y - c_s)^p}{(x - c_s)^p} \end{aligned} \quad (2.7)$$

where the series converges for $|y - c_s| < |x - c_s|$. We note (2.7) is exactly of the form required with $C_p(y) = -\frac{1}{p}(y - c_s)^p$ and $B_p(x) = (x - c_s)^{-p}$. We define a 'multipole expansion' of the charges in Ω_s as a vector $\hat{\mathbf{q}}^s = \{\hat{q}_p^s\}_{p=0}^{P-1}$,

$$\begin{cases} \hat{q}_0^s = \sum_{j \in I_s} q_j \\ \hat{q}_p^s = \sum_{j \in I_s} -\frac{1}{p} (x_j - c_s)^p q_j, \quad p = 1, 2, 3, \dots, P-1 \end{cases} \quad (2.8)$$

The multipole expansion is a representation of the charges in Ω_s and can be truncated to any required precision. We can use the multipole expansion in place of a direct calculation with the particles in Ω_s . As the potential in Ω_t can be written as,

$$\phi(x) = \sum_{j \in I_s} K(x, y) q_j = \log(x - c_s) \hat{q}_0^s + \sum_{p=1}^{\infty} \frac{1}{(x - c_s)^p} \hat{q}_p^s \quad (2.9)$$

Greengard and Rokhlin also define a local expansion centered on Ω_t , that represents the potential due to the sources in Ω_s .

$$\phi(x) = \sum_{l=1}^{\infty} (x - c_t)^l \hat{\phi}_l^t \quad (2.10)$$

with a simple computation to derive the local expansion coefficients $\{\hat{\phi}_p^t\}_{p=0}^{\infty}$ from $\{\hat{q}_p^s\}_{p=0}^{P-1}$ (see app. A).

For our purposes it's useful to write the multipole expansion in linear algebraic terms as a linear map between vectors,

$$\hat{\mathbf{q}}^s = \mathbf{T}_s^{P2M} \mathbf{q}(I_s) \quad (2.11)$$

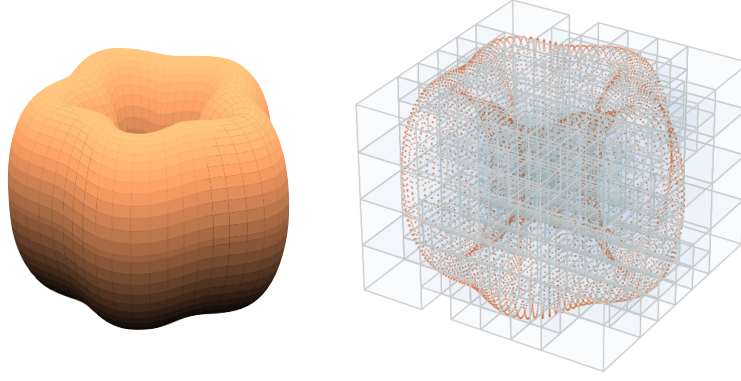


Figure 2.2: An adaptive octree for random point data placed on the surface of a ‘wiggly torus’ test geometry. The user defines the level of recursion via a threshold for the maximum number of particles in a given node.

where \mathbb{T}_s^{P2M} is a $P \times N_s$ matrix, analogously for the local expansion coefficients we can write,

$$\hat{\phi}^t = \mathbb{T}_{t,s}^{M2L} \hat{\mathbf{q}}^s \quad (2.12)$$

where $\mathbb{T}_{t,s}^{M2L}$ is a $P \times P$ matrix, and the calculation of the final potentials as,

$$\phi^t = \mathbb{T}_t^{L2P} \hat{\phi}^t \quad (2.13)$$

where \mathbb{T}_t^{L2P} is a $N_t \times P$ matrix. Here we denote each *translation* operator, \mathbb{T}^{X2Y} , with a label read as ‘ X to Y ’ where L stands for local, M for multipole and P for particle. Written in this form, we observe that one could use a different method to approximate the translation operators than explicit kernel expansions to recover our approach’s algorithmic complexity, and this is indeed the main difference between different implementations of the FMM.

We have described how to obtain linear complexity when considering two isolated boxes, however in order to recover this for interactions between *all particles* we rely on a hierarchical partitioning of Ω using a data structure from computer science called a *quadtree* in \mathbb{R}^2 or an *octree* in \mathbb{R}^3 . The defining feature of these data structures is a recursive partition of a bounding box drawn over the region of interest (see fig. 2.2). This ‘root node/box’ is subdivided into four equal parts in \mathbb{R}^2 and eight equal parts in \mathbb{R}^3 . These ‘child nodes/boxes’ turn are in turn recursively subdivided until a user defined threshold is reached based on the maximum number of points per leaf box. These trees can be ‘adaptive’ by allowing for non-uniform leaf box sizes, and ‘balanced’ to enforce a maximum size constraint between adjacent leaf boxes [37].

In addition to the \mathbb{T}^{P2M} , \mathbb{T}^{M2L} and \mathbb{T}^{L2P} the FMM also require operators that can translate the expansion centre of a multipole or local expansion, \mathbb{T}^{L2L} , \mathbb{T}^{M2M} , an operator that can add the contribution of a set of points to a given local expansion \mathbb{T}^{P2L} , and apply a multipole approximation to a set of points, \mathbb{T}^{M2P} , finally we need define a $P2P$ operator, which is short hand for direct kernel evaluations. Algorithm (3) in Appendix C provides a sketch of the full FMM algorithm which combines these operators.

In summary the algorithm consists of two basic steps. During the first step, the upward pass, the tree is traversed in post-order¹. At the leaves, multipole expansions are built using T^{P2M} . At each non-leaf box, the multipole expansions are shifted to the box's centre from its children using T^{M2M} and summed. In the second step, the downward pass, the tree is traversed in pre-order². The local expansions are computed by first translating the multipole expansions of boxes which are the children of the parents of a box, but are not adjacent to it, using T^{M2L} and are summed, a second contribution is found from a box's parent using T^{L2L} to shift the expansion centre from a box's parent to its own centre. It is common to refer to boxes for which T^{M2L} is applied to for a given box B as its *interaction list*. The sum of these two parts encodes all the contribution from sources particles in boxes with are not adjacent to itself. For non-uniform trees there also may be a contribution from boxes in near field of B , i.e. neighbour children/descendants, calculated using T^{P2L} . This is computed at the leaf level only. Having assembled the far-field contribution at B in its local expansion we evaluate it at the particles it contains using T^{L2P} , combining it with its near interactions from particles in adjacent boxes using $P2P$, as well as boxes which are non-adjacent but for which the multipole expansion still applies using T^{M2P} in a box's near-field, i.e. the children and descendants of adjacent boxes at the same level.

The complexity bound of the FMM algorithm is due to the hierarchical nature of the data structure used in its computation. In the upward pass, each box only considers either itself. This leads to a complexity of $O(N)$, as the number of leaf boxes is bounded by the number of particles. In the downward pass, the number of boxes each box considers when computing translations is bounded by the number of non-adjacent children of its parent box for the T^{M2L} step, i.e. the size of its interaction list. As this is a constant (27 in \mathbb{R}^2 and 189 in \mathbb{R}^3), this step is again $O(N)$ in complexity, resulting in a total complexity of $O(N)$ for this step. In the T^{L2L} and T^{L2P} operators each box considers only itself. For the leaf level computations, the $P2P$, T^{P2L} and T^{M2P} steps are bounded to be contained in boxes in B 's near field³. This leads to an overall algorithmic complexity of $O(N)$. We note that this complexity bound is entirely dependent on the properties of the kernel. Highly oscillatory kernels are not as rank-deficient, however corresponding algorithms inspired by the FMM have been developed for them, however here the complexity increases to $O(N \log(N))$ [27]. The conversion of an $O(N^2)$ problem to one that can be solved in $O(N)$ was a groundbreaking discovery, and lead to the admissibility of a large number of scientific problems to computer simulation. As a result the FMM has been described as 'one of the top ten algorithmic discoveries of the twentieth century', taking its place alongside revolutionary algorithms such as Quicksort and the Fast Fourier Transform (FFT) [10].

2.2 Algebraic FMM Variants

In its original analytical form the applicability of the FMM is limited by the requirement for an explicit multipole and local expansions, as well as a restriction to matrix vector products. Subsequent decades saw the development of 'algebraic'

¹The children of a box are visited before the box itself.

²The children of a box are visited after the box itself.

³In the worst case, for highly non-uniform point distributions, these steps can be subsumed into the $P2P$ step, allowing us to maintain the bound.

analogues to the original algorithm. These methods are similarly based on a hierarchical partitioning, whether that be of the point data using a recursive tree as with the original FMM [24, 12], or by operating on the matrix implied by the FMM's algorithmic structure directly [15, 7, 9]. The latter methods are collectively known as \mathcal{H} -matrix methods. Representing the FMM operation in this way has allowed extension of the FMM to other matrix computations, such as matrix-matrix products, as well as approximations of its inverse [1]. Notably, many of these methods don't necessarily rely on explicit multipole/local expansions for approximating fields as in the original FMM in the previous section. Examples such as the 'kernel independent FMM' (kiFMM) of Ying and co-authors instead relies on the method of fundamental solutions to approximate the fields and requires only evaluating kernel values, and is applicable to a wide range of kernels from second-order linear non-oscillatory elliptic PDEs with constant coefficients such as the Laplace equation. This approach relies on some analytic considerations, however methods also exist which are interpolatory - such as the 'black box FMM' (bbFMM) of Fong and Darve [12], which similarly only relies on kernel evaluations and a Chebyshev scheme to approximate fields.

In our software we choose to implement the kiFMM of Ying and coauthors, which we explain in detail below adapting the discussion from Section 3 of [24]. This method shares advantages with other algebraic FMM methods, of generality to a large class of problems, as well as opportunities to optimise computer implementations we explore in Section 2.2. This approach relies on a spatial discretisation of the problem domain via an quad/octree as in the original FMM, as well as the method of fundamental solutions (MFS) for approximating the fields from point charges/masses. This method has been demonstrated to perform well on shared memory systems [43], achieve similar accuracy to the analytical variant, with relatively low pre-computation required⁴. The underlying data structure of the quad/octree has been a significant area of research and development, with established high-performance methods for their construction in shared/distributed memory environments [37, 36, 8].

Consider the kernels for second-order constant coefficient non-oscillatory PDEs, such as that of the Laplace equation in (2.2). Such kernels satisfy the underlying PDE everywhere except the singularity location, and are smooth away from this singularity. These problems admit a unique solution for interior/exterior Dirichlet boundary value problems (see Appendix D for a demonstration of this for the Laplace equation). The authors of [24] rely on the smoothness and uniqueness of the Dirichlet boundary value problems as basic properties to develop their FMM formulation. The problem setting as before is the calculation of (2.1) for the Laplace kernel, for a set of N point sources y_i , $i = 1 \dots N$, which we will associated with N source densities q_i , an target locations y_j , $j = 1 \dots M$. As before, the source and target locations may coincide. We use an index set I_s^B and I_t^B to identify the sources and targets we are considering in a particular interaction. We assume that our problem is in \mathbb{R}^3 , however the exposition is essentially the same as in \mathbb{R}^2 .

Assuming that we have constructed our hierarchical tree partitioning, which may be adaptive, the first step is to approximate the fields due to particles contained in each leaf box. We specify more concretely that for a given box, B , its 'near field range', \mathcal{N}^B , is the set of 27 boxes at the same level of a tree which are adjacent to it, i.e. they share a corner, face or edge as well as B itself. Its 'far field range', \mathcal{F}^B , is simply the boxes which are the complement of this.

We approximate the potential in \mathcal{F}^B from the source densities $\{q_i : i \in B\}$ in

⁴This depends heavily on the choice of how to sparsify T^{M2L} , see Section 3.2.2 for more details.

B using the potential from an *equivalent density distribution*, $q^{B,u}$, supported at prescribed locations $y^{B,u}$ (see the left box in Figure 2.3). Where $q^{B,u}$ is called the *upward equivalent density* and $y^{B,u}$ is called the *upward equivalent surface*. This amounts to representing the potential with a ‘single layer’ potential [20],

$$\phi(x) := \int_{y \in y^{B,u}} q^{B,u}(y) K(x, y) ds(y), \quad x \in \mathbb{R}^3 \setminus y^{B,u} \quad (2.14)$$

To guarantee the smoothness of the potential produced by $q^{B,u}$ in the far-field, its support $y^{B,u}$ must not overlap with \mathcal{F}^B due to the singularities in this integral from the kernel function when evaluated on the equivalent surface. Secondly, we note that the equivalent surface must enclose B from the definition of the single layer potential [20]. We see that the equivalent surface must be placed in between the box and the boundary of \mathcal{F}^B .

The potential induced by our equivalent densities and upward equivalent surface satisfies the Laplace equation. Therefore, due to the uniqueness of the exterior Dirichlet boundary value problem for this kernel (as well of kernels of a similar type), we reason that the potential calculated using (2.1) directly from the source particles must be equivalent to that calculated using (2.14) in \mathcal{F}^B , or anywhere between $y^{B,u}$ and \mathcal{F}^B . Thus we place an intermediate surface called the *upward check surface* between \mathcal{F}^B and $y^{B,u}$, denoting it with $x^{B,u}$. The potential computed at this surface is called the *upward check potential*, which we denote by $\phi^{B,u}$.

We write this as,

$$\int_{y^{B,u}} K(x, y) q^{B,u} dy = \sum_{i \in I_s^B} K(x, y_i) q_i = \phi^{B,u}, \text{ for any } x \in x^{B,u} \quad (2.15)$$

Solving for the equivalent densities is an equivalent method of approximating the far-field potential induced by the points in B . We identify this with a *multipole expansion*. Now considering source densities which are not contained in a box B (see right box of Figure 2.3) but in its \mathcal{F}^B , we can construct an equivalence for local expansions using a similar approach. To ensure the existence of the *downward equivalent densities* $q^{B,d}$, the *downward equivalent surface*, $y^{B,d}$, must be located between B and \mathcal{F}^B and the potentials generated by the source points are matched to those generated by the equivalent points on a *downward check surface*, $x^{B,d}$ that encloses the box and is itself enclosed by $y^{B,d}$ in order to calculate a *downward check potential* $\phi^{B,d}$.

$$\int_{y^{B,d}} K(x, y) q^{B,d} dy = \sum_{i \in I_s^{\mathcal{F}^B}} K(x, y_i) q_i = \phi^{B,d} \text{ for any } x \in x^{B,d} \quad (2.16)$$

In \mathbb{R}^3 the authors chose to represent the equivalent and check surfaces as cubes, with the equivalent/check points arranged regularly over the surfaces. We choose the same as it leads to implementation benefits when designing the field translation operators (see Section 3.2.2 for how we take advantage of this).

Equations (2.15) and (2.16) are examples of *Fredholm integral equations of the first kind*, the inversion of which is ill-posed. To solve these equations, we must first discretise, for which we made use of the *Method of Fundamental Solutions* (MFS), a

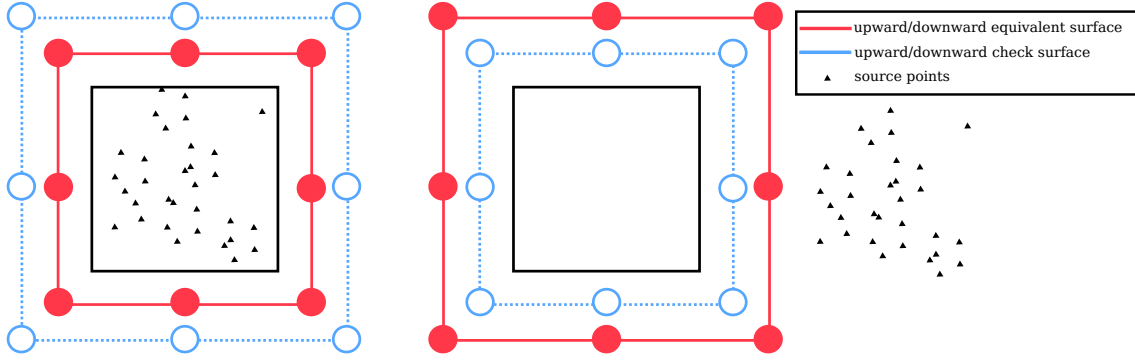


Figure 2.3: We illustrate the equivalent/check surfaces and associated boxes in \mathbb{R}^3 , where we show a corresponding cross section. In the first figure, we illustrate the situation in the ‘P2M’ operation, where we are trying to construct an approximation to the potential generated by points in a box by matching it to that generated by a set of equivalent density points placed on a fictitious surface enclosing it. In the second figure we illustrate the ‘P2L’ operation, where we are now trying to construct an approximation to the potential generated by points in a box’s far-field within the box.

technique whereby the potential is approximated by a linear combination of kernel function evaluations at a set of discrete points with associated densities,

$$\phi(x) \approx \phi^N(x) = \sum_{y_i \in y^{B,u}} K(x, y_i) q_i \quad (2.17)$$

Where N denotes the number of equivalent points of density are placed on the equivalent surface. To see how this approximates the single-layer operator we used above to calculate the potential we simply replace the continuous density functions in (2.14) with $\sum_{j=1}^N q_j \delta(y - y_j)$, recovering (2.17). Writing (2.15) or (2.16) in matrix form reflecting the discretisation via MFS,

$$Kq = \phi \quad (2.18)$$

We can solve the problem with Tikhonov regularisation,

$$q = (\alpha I + K^* K)^{-1} K^* \phi \quad (2.19)$$

which converts it into a *Fredholm integral equation of the second kind* which are well-posed. The regularisation parameter α is found empirically. Computing (2.15) is equivalent to the T^{P2M} operator described in the previous section for the analytical FMM, (2.16) is equivalent to an T^{P2L} operator which was not explicitly described. As before, these operators take a set of charges, and create expansions that allow us to evaluate their potential in the far-field, however the method of creating the expansions is clearly significantly different. The most notable change being that our above formulation *does not require explicit analytical expansions of the kernel function*, only making use of kernel evaluations.

To complete the kiFMM we need analogues to the field translation operators, T^{M2L} , T^{M2M} , T^{L2L} . We illustrate the required surfaces for each of these operators

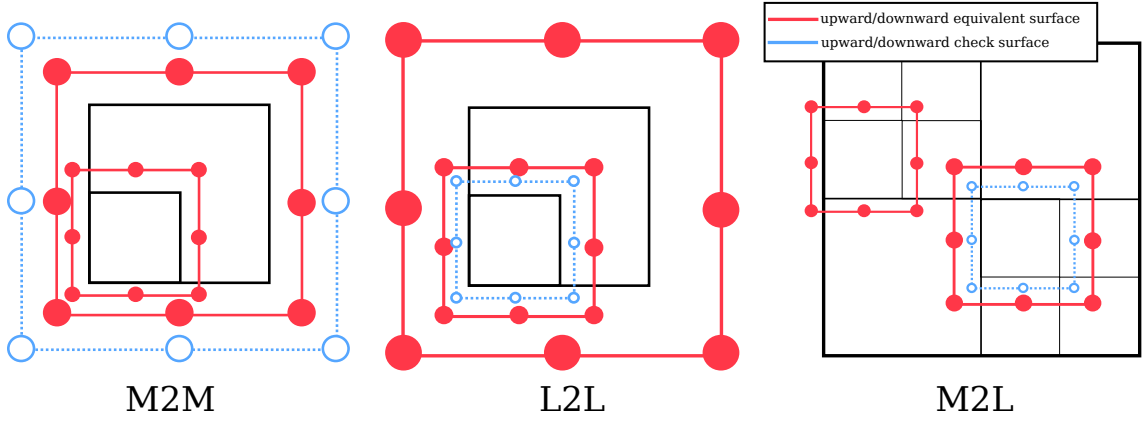


Figure 2.4: As in Figure 2.3, we illustrate the translations as cross sections of the surfaces, which are cubes in \mathbb{R}^3 .

in Figure 2.4. For T^{M2M} we must translate the upward equivalent density of A to the centre of its parent box B , solving the following equation for $q^{B,u}$,

$$\int_{y^{B,u}} K(x, y) q^{B,u}(y) dy = \int_{y^{A,u}} K(x, y) q^{A,u}(y) dy, \text{ for all } x \in x^{B,u} \quad (2.20)$$

As before, $y^{A,u}$ must enclose the child box A . During the downward pass, we must evaluate the downward equivalent density, corresponding to a local expansion, from the multipole expansions of non-adjacent boxes in B 's parent neighbour's children. We similarly write down for T^{M2L} ,

$$\int_{y^{B,d}} K(x, y) q^{B,d}(y) dy = \int_{y^{A,u}} K(x, y) q^{A,u}(y) dy, \text{ for all } x \in x^{B,d} \quad (2.21)$$

Finally, the local expansions of each box B must be translated to the centre of each of its children A ,

$$\int_{y^{B,d}} K(x, y) q^{B,d}(y) dy = \int_{y^{A,d}} K(x, y) q^{A,d}(y) dy, \text{ for all } x \in x^{B,d} \quad (2.22)$$

For each of these translation operators we use the discretisation based on MFS discussed above, and solve using Tikhonov regularisation. For the T^{L2P} , $P2P$ and T^{M2P} operators we simply use direct kernel evaluations at the target points with respect to the equivalent densities represented by the multipole or local expansion coefficients or the true densities at the source points.

2.3 Implementation Challenges for the Kernel Independent Fast Multipole Method

In this section we introduce analytical features of the kernels compatible with the kiFMM that have consequences for computer implementations, such as the ability to pre-compute and cache matrices that correspond to translation operators. We also discuss the octree data structure in more detail, highlighting its key bottlenecks, concluding with a discussion on implied computational and storage complexity.

The defining feature of the kernels compatible with the FMM is that they display a rapid decay behaviour as the distance between interactions increases, known formally as *asymptotic smoothness*. A kernel is described as asymptotically smooth if there are constants $C_{as1}, C_{as2} \in \mathbb{R}_{>0}$ that satisfy,

$$\|\partial_x^\alpha \partial_y^\beta K(x, y)\| \leq C_{as1}(C_{as2}\|x - y\|_2)^{-|\alpha| - |\beta|} \alpha + \beta |K(x, y)| \quad (2.23)$$

for all multi-indices $\alpha, \beta \in \mathbb{N}_0^3$ and all $x, y \in \mathbb{R}^3$. It's this smoothness that allows us to limit the definition of \mathcal{N}^B to its neighbouring boxes in the FMM. Considering the situation in \mathbb{R}^3 only, this leads to $|\mathcal{N}^B| = 3^3 = 27$.

Far-field interactions are handled by the T^{M2L} step, we saw above how this is limited to interactions with boxes which are children of B 's parent, but non-adjacent to B . Therefore we see that in a multi-level scheme the \mathcal{N}^B contains all of the $6^3 = 216$ near and far field interactions of B 's children. As far-field interactions necessarily exclude the near field, this leads to a maximum of $6^3 - 3^3 = 189$ boxes in each child box's far field that must be considered, each corresponding to a single T^{M2L} . This is one of the *key bottlenecks* of efficient FMM implementations. There are numerous ways of *sparsifying* this step, either by using some additional numerical technique such as an SVD to compress the matrices corresponding to T^{M2L} as they are known to be low-rank, or by using an exact method such as an Fast Fourier Transform (FFT) - which relies on our decision to place the equivalent densities on a regular grid as then the T^{M2L} can be re-interpreted as a convolution. We discuss the trade-offs of these approaches in detail in Section 3.2.2, as optimal implementations of this sparsification are of central importance to our software's performance.

We note that precomputations can be further reduced if kernels also exhibit translational invariance,

$$K(x, y) = K(x + v, y + v) \quad (2.24)$$

where $v \in \mathbb{R}^3$, we can compute T^{M2L} for a restricted subset of the total possible interactions for the eight child boxes. Indeed, the union of all possible far-field interactions for the eight child boxes gives $7^3 - 3^3 = 316$ possible interactions. This comes from the fact some subset of translation vectors are non-overlapping for each child, resulting in a total of 7^3 total interactions for all children, subtracting the near-field interactions which are the same for all children gives the result. Furthermore this means that we must pre-compute just 316 unique T^{M2L} if our kernel has these favourable properties. This is of course dependent on choosing the same equivalent and check surfaces, and density locations, for each box. If so, these can be pre-computed and cached for a given expansion order, corresponding to all possible T^{M2L} at each level.

If an asymptotically smooth, translationally invariant, kernel is also homogeneous to degree n ,

$$K(\alpha r) = \alpha^n K(r) \quad (2.25)$$

where $\alpha \in \mathbb{R}$, implies that when we scale the distance between a source and target box by α the potential is scaled by a factor of α^n , where n depends on the kernel function in question, we can compute T^{M2L} for a *single* level of the tree, and scale the result at subsequent levels. This is summarised in Table 2.1.

Table 2.1: Number of near and far field boxes for a given box B , depending on the type of kernel we’re considering.

Kernel Type	boxes in \mathcal{N}^B	boxes in \mathcal{F}^B
trans. invar.	≤ 27 per box	≤ 316 per level
trans. invar. + homog.	≤ 27 per box	≤ 316 in total

As we’ve chosen the location of point densities to be fixed relative to each box, the evaluation of (2.20) and (2.22) can equivalently be pre-computed. In this case, there are just 8 unique matrices corresponding to T^{M2M} and T^{L2L} , corresponding to the relative positions between a parent box and its children.

We observe the T^{P2M} is calculated for all the nodes of a quad/octree in a discretisation, as observed in the previous section the level of discretisation is either specified by the user, or set by a user defined constraint N_{crit} which specifies a maximum number of points contained within each leaf box. This leads to $O(N \cdot N_{\text{crit}})$ to find the check potentials for each leaf, therefore we note that N_{crit} must be kept small to ensure linear complexity is maintained for this operation. To compute the equivalent density, we rely on an application of the inverted integral operator in (2.15). The size of this matrix is determined by the expansion order P , which determines the number of quadrature points taken on the equivalent/check surfaces. As the points are taken to be placed on a regular grid over this surface, the number of quadrature points N_{quad} relates to P as,

$$N_{\text{quad}} = 6(P - 1)^2 + 2 \quad (2.26)$$

Therefore, this matrix vector product is of $O((P - 1)^4)$, leading to $O(N((P - 1)^4 + N_{\text{crit}}))$ complexity for the entire operator. The complexity of T^{P2L} is the same, as it amounts to the same calculation, albeit to form a local expansion. The pre-computation of the translation operator requires an SVD for the integral operator in (2.15), the complexity of which is dependent on the algorithm chosen, with implementation specific optimisations. However, for a $\mathbb{R}^{m \times n}$ matrix where m and n are of similar size, the ‘DGESVD’ implementation of LAPACK, which we use in our software framework, has a complexity of $O(n^3)$ therefore this precomputation is of $O((P - 1)^6)$. The storage required is of $O((P - 1)^4)$ for the inverted matrix.

Applying similar analysis for computing (2.20) and (2.22), we arrive at computational complexities of $O(N \cdot (P - 1)^4)$ for calculating the check potentials, and then evaluating the equivalent densities via two matrix-vector products. For the M2L step, if we do not choose to implement any sparsification, we also obtain $O(N \cdot (P - 1)^4)$ for the asymptotic complexity of applying T^{M2L} , however here there are large lurking constants. Specifically, each box B has to apply an T^{M2L} up to 189 times in \mathbb{R}^3 or 27 times in \mathbb{R}^2 . The storage complexity is determined by the kernel, as shown by table 2.1, the properties of the kernel can reduce the number of precomputations that can be cached.

Similar large constants lurk in the leaf level computations $P2P$, T^{M2P} , T^{P2L} . These all consider boxes contained in B ’s near field. For non-uniform point distribution there could be very large number of boxes contained in the near field. Therefore to reduce this we enforce a ‘balancing’ condition, as mentioned above. The most common condition is a ‘2:1 balance’, whereby neighbouring boxes are restricted to be no more than twice as large as each other [25]. This restricts the

size of the number of adjacent boxes to B to be at most 52 in \mathbb{R}^3 . For these boxes we will calculate the potential for points in B using kernel evaluations directly via $P2P$. For the remainder of its near field, we'll use the T^{M2P} operator. This operator considers boxes in B' near field for which the multipole expansion still applies at B , this means that leaf boxes that coincide with B 's neighbours children that are non-adjacent to B . At most there are 156 such boxes in \mathbb{R}^3 . There may also be an additional contribution to the local expansion at B not captured in T^{L2L} and T^{M2L} , from boxes in the near-field of B 's parent which are the leaf level, and considered in the far-field of B itself, and are the level of B 's parent. These contributions are found via T^{P2L} . With our balancing condition there are at most 19 such boxes in \mathbb{R}^3 . We note that for uniformly refined trees T^{M2P} and T^{P2L} aren't calculated as their corresponding interactions are subsumed into $P2P$. The $P2P$ operator is therefore of $O(52N \cdot N_{\text{crit}})$, with no storage cost as this is applied directly to points. Similarly, the complexity of T^{M2P} is $O(156N \cdot (P-1)^2 N_{\text{crit}})$, T^{L2P} is of $O(N(P-1)^2 \cdot N_{\text{crit}})$. The complexity of T^{P2L} is $O(19N \cdot ((P-1)^4 + N_{\text{crit}}))$, where we include the cost of calculating the check potential as in T^{P2M} . The complexities of each step are summarised in table 2.2. These complexities are only an upper bound, for T^{M2P} and T^{P2L} , and correspond to quite extreme point distributions, rarely occurring for all boxes in a given discretisation. In practice these are found to be an order of magnitude smaller than the number of boxes that must be considered in T^{M2L} for point distributions that are relatively uniform ⁵.

Therefore the largest bottlenecks are the $P2P$ and T^{M2L} steps, and the area of focus in optimised implementations. When implemented naively, T^{M2L} contains a large number of BLAS level 2 operations, and is calculated for every non-leaf box below the first level of an octree/quadtree. An obvious optimisation is to re-order data such that a single BLAS level 3 operation is computed for each box. This increases the ratio of computations to memory accesses by converting a series of matrix-vectors product into a single matrix-matrix product for each box. Additionally, the SVD taken for the integral operators above can be cut-off due to the low-rank nature of the above operators, leading to a reduced storage and application complexity. We explore the rank behaviour in more detail in Chapter 3.2.2 for the Laplace kernel. If instead one chooses to take an FFT, which offers lower complexity for each T^{M2L} while being an exact translation, one has to compute the FFT corresponding to each unique translation which as we've seen is kernel dependent, and perform an inverse FFT to evaluate the check potentials at the equivalent density points. This leads to a lower overall complexity for both compute and storage - however, as we observe in Section 3.2.2, memory accesses are critical to performant implementations. The performance of the $P2P$, T^{M2P} and T^{L2P} operators are determined most significantly by the ability to rapidly evaluate the kernel function over sets of points. This is a ripe area for compute optimisations, such as GPU off-loading, or developing vectorised CPU code, and is therefore highly-dependent on the available computational resources and their respective architectures. Practical implementations should be flexible enough to for developers to 'plug-in' different implementations in order to experiment with new hardware.

The second major bottleneck with the kiFMM and FMMs more generally, especially in a distributed setting, is the quad/octree data structure. The tree is crucial to performance as being able to rapidly query, and communicate via the tree, especially in a distributed setting will determine the overall runtime, as communication

⁵For example for randomly distributed on the surface of a sphere, or normally distributed points, typical values are $O(10)$ boxes for T^{M2P} and $O(1)$ boxes for T^{L2P}

Table 2.2: Asmyptotic complexities of each kiFMM operator in \mathbb{R}^3 , with constants left to demonstrate relative contrast. For T^{M2L} we provide a few different complexity estimates, starting with ‘naive’ implementation which applies the inverted integral equation (2.21) up to 189 for each box as a matrix vector product, with no sparsification. Then the complexities with respect to different kernel properties. For an T^{M2L} sparsified via the SVD we indicate a cut-off rank with κ , for an FFT based approach as we are often working with real data for the densities we can retain only half the calculated frequencies to save on storage costs. For the T^{P2L} , T^{M2P} and $P2P$ operators we provide estimates for 2:1 balanced trees, as we restrict ourselves to this a practical implementation.

Operator	Computational Complexity	Storage Complexity
T^{P2M}	$O(N(36(P-1)^4 + N_{\text{crit}}))$	$O(36(P-1)^4)$
T^{M2M}	$O(36N(P-1)^4)$	$O(8 \cdot 36(P-1)^4)$
T^{L2L}	$O(36N(P-1)^4)$	$O(8 \cdot 36(P-1)^4)$
T_{naive}^{M2L}	$O(189N \cdot 36(P-1)^4)$	$O(189N \cdot 36(P-1)^4)$
$T_{\text{trans. inv.}}^{M2L}$	$O(189N \cdot 36(P-1)^4)$	$O(316 \log(N) \cdot 36(P-1)^4)$
$T_{\text{homog+trans. inv.}}^{M2L}$	$O(189N \cdot 36(P-1)^4)$	$O(316 \cdot 36(P-1)^4)$
$T_{\text{homog+trans. inv. + SVD}}^{M2L}$	$O(189N \cdot 6(P-1)^2 \cdot \kappa)$	$O(316 \cdot 6(P-1)^2 \cdot \kappa)$
$T_{\text{homog+trans. inv. + FFT}}^{M2L}$	$O(189N \cdot 4(P-1) \log(P-1))$	$O(316 \cdot 36(P-1)^4)$
$T_{\text{homog+trans. inv. + Real FFT}}^{M2L}$	$O(189N \cdot 4(P-1) \log(P-1))$	$O(316 \cdot 18(P-1)^4)$
T^{L2P}	$O(N(36(P-1)^4 + N_{\text{crit}}))$	$O(1)$
$T_{\text{balanced}}^{P2L}$	$O(19N \cdot (36(P-1)^4 + N_{\text{crit}}))$	$O(1)$
$T_{\text{balanced}}^{M2P}$	$O(156N \cdot (36(P-1)^4))$	$O(1)$
$P2P_{\text{balanced}}$	$O(52N \cdot N_{\text{crit}})$	$O(1)$

latency is a leading order variable in the distributed FMM’s complexity [44]. Though there has been significant scholarship in developing high-performance tree libraries for parallel and distributed settings [8, 37, 36], we observe that relatively little work has been done to examine and develop tree libraries with the FMM explicitly in mind, we explore potential optimisations in Section 3.1.1. Specifically, T^{M2M} summarises global information that is required by each box, and is later distributed via T^{M2L} this necessarily involve communication across node boundaries in a distributed setting. Additionally, the broad applicability of parallel trees necessitates a design of software that is relatively de-coupled from the FMM code to encourage adoption in other communities. These two concerns determine the implementation strategy of our own tree library.

2.4 Building for Re-Use in Fast Algorithm Software

High performance software for the core data structure of quad/octrees is essential to all fast algorithms. Indeed, these hierarchical discretisations of space find applica-

tions across scientific computing when modelling multi-scale phenomena. Similarly, methods for sparsifying the T^{M2L} operator, whether that be via an SVD or FFT, can also be re-used in the implementation of fast direct solvers, or alternative algebraic FMMs such as the bbFMM of Fong and Darve [12]. The same is true of software for evaluating kernel functions in the $P2P$ operator. We identify the decoupling of separate sub-components to be rare in other softwares for fast algorithms [25, 43, 6], which are often presented as a monolith to users, making it difficult for developers to extend or adapt this software to their use-case.

Software engineering practice, traditionally object oriented programming, is centered on a set of key principles known via an acronym SOLID⁶. In this section we explain how some of Rust’s features allow us to enforce ‘S’ - the ‘single responsibility’ principle, as well as ‘O’, the ‘open close’ principle, and the ‘D’ - dependency inversion principle, of SOLID which allow us to create software for fast algorithms that is composed of sub-components that are easy to modify and extend, and usable from downstream projects that may want to utilise a subset of our software’s functionality.

Beginning with the ‘single responsibility’ principle. Cargo’s ‘workspaces’ feature allows all sub-packages (known as ‘crates’ in Rust) to share a common build directory, speeding up build compile times for shared dependencies and ensuring that dependencies are uniformly versioned across all crates, specified by a root level TOML dependency file. Indeed, crates within a workspace can be specified to be binaries, libraries, or both, allowing for sub-components to easily be deployed independently or used as a dependency by a downstream developer. This allows for example users to make use of sub-components such as our tree library, or implementation of kernels, without having to install an FMM implementation that relies upon it.

Rust’s trait system is designed to enforce the open/close principle. As we’ve seen above, FMM implementations can depart quite radically from that originally presented by Greengard and Rokhlin, despite sharing a common algorithmic structure, or data structure. In designing our software we want to build a platform to rapidly add functionality, and compare performance. For example, if we can design an alternative $P2P$ operator that uses a GPU, or wanted to contrast methods to sparsify T^{M2L} such as the SVD or FFT approaches mentioned above it should be possible to leave the remainder of our kiFMM intact. If we wanted to entirely replace the kiFMM by an equivalent alternative, such as the bbFMM or the original analytical FMM, and re-use the distributed octrees, the kernel evaluations, and the general algorithmic structure it should also be possible to do so. Indeed, the difficulty in comparing directly methods to sparsify T^{M2L} or the relative performance of two algebraic FMM approaches comes down to the diversity in their respective implementations as presented by the authors, making it difficult to isolate independent variables that can explain performance differences in terms of speed or accuracy. To compare the relative merits of Trait based design over object oriented design, let’s take the example of building an abstraction for an FMM implementation in our software.

We begin by defining a trait for FMM algorithms, which we choose to make as

⁶S - single responsibility, a software unit is responsible for a quantum of functionality. O - Open/close principle, whereby extensions should be easy, but presented software is closed for modification. L - Liskov substitution, a software class should be replaceable with a sub-class without breaking the software. I - Interfaces should be segregated such that code relying on them shouldn’t depend on methods it doesn’t use. D - Dependency inversion, high-level modules should not have to worry about low level implementation details

general as possible so we can specialise it for different algorithms, distributed or single node trees, or expansion orders.

```

1 use bempp::traits::kernel::Kernel;
2 use bempp::traits::tree::Tree;
3
4 pub trait Fmm {
5     // Associated type for a kernel
6     type Kernel: Kernel;
7
8     // Associated type for a tree
9     type Tree: Tree;
10
11     // Expansion order
12     fn order(&self) -> usize;
13
14     // The kernel function
15     fn kernel(&self) -> &Self::Kernel;
16
17     // The tree (single node or distributed)
18     fn tree(&self) -> &Self::Tree;
19 }

```

Listing 2.1: Traits for FMM Algorithms.

To read the code in Listing 2.1, we introduce a Rust language feature known as an ‘associated’ type. This amounts to a placeholder which can be populated by an implementer. Associated types can be constrained to have certain behaviour, in this case we’ve enforced our associated types to have ‘Trait bounds’, i.e. we expect the placeholders to implement the interface specified by two other Traits, specifically Traits that specify how a Kernel and a Tree should behave. Our Kernel Trait contains methods for single and multithreaded kernel evaluations, as well as assembly of Kernel matrices corresponding to the interactions between sets of sources and points⁷, similarly our Tree Trait is generic over single/multi-nodes - just specifying the behaviour to query boxes and the points that they may contain⁸. Each Trait is implemented by a concrete type created by a user, for example a struct, and defines an *interface* which must be implemented by the type. Rust traits from foreign libraries can be implemented for local types only, this is to avoid situations in which traits are re-implemented by downstream users of software that may be implemented by the libraries developers.

We see here that the Traits do not specify how the data for our FMM looks like, this allows us to specialise for different implementations such as the kiFMM as follows. We begin by creating an interface for T^{M2L} shown in Listing 2.2. Notice the generic parameters after the name of the trait ‘T’, which is constrained to behave in accordance with the Kernel Trait. There are two traits here, one specifying how data should be accessed for a given T^{M2L} implementation, and another providing an interface to call the operator over the boxes in a given level of a tree. We use this pattern of separating the interface for data access from that for the operator to give us flexibility in exactly how the data corresponding to T^{M2L} is stored in practice. For example, an SVD based operator would store data of a different shape to an FFT based one, alongside different meta-data required for its application. The

⁷<https://github.com/bempp/bempp-rs/blob/feat/rlst-fmm/traits/src/kernel.rs>

⁸<https://github.com/bempp/bempp-rs/blob/feat/rlst-fmm/traits/src/tree.rs>

first Trait simply specifies that a user must be able to call methods to precompute the operators for a given kernel function, which as we saw in the previous section has implications for the amount of pre-computation possible, as well as for a given domain - which may be distributed.

```

1 use bempp::traits::kernel::Kernel;
2
3 pub trait FieldTranslationData<T>
4 where
5     T: Kernel,
6 {
7     // An associated type for the relative position between
8     // two boxes
9     type TransferVector;
10
11     // An associated type for how the M2L operators may look
12     // after sparsification
13     type M2LOperators;
14
15     // The type of domain, which may be single node/
16     // distributed
17     type Domain;
18
19     // Compute unique transfer vectors
20     fn compute_transfer_vectors(&self) -> Self::
21     TransferVector;
22
23     // Precompute the field translation operators
24     fn compute_m2l_operators(
25         &self,
26         expansion_order: usize,
27         domain: Self::Domain,
28         // );
29     ) -> Self::M2LOperators;
30
31     // Number of coefficients for a given expansion order
32     fn ncoeffs(&self, expansion_order: usize) -> usize;
33 }
34
35 pub trait FieldTranslation {
36     // How to scale operator with tree level.
37     fn m2l_scale(&self, level: u64) -> f64;
38
39     // Field translation operation over each level.
40     fn m2l(&self, level: u64);
41 }

```

Listing 2.2: Trait for Multipole to Local Field Translation

A concrete implementation for a given algorithm such as the kiFMM then requires two structs one to hold the data and another to specify the concrete implementation of an FMM algorithm by containing a reference to the type of tree, kernel and T^{M2L} method used. This is shown in Listing 2.3. In this listing we have a few more generic parameters, constraining the corresponding associated types to behave as specified by these Traits.

```

1 pub struct KiFmm<T: Tree, U: Kernel, V: FieldTranslationData<
    U>> {
2
3     // The expansion order of multipole and local expansions.
4     pub expansion_order: usize,
5
6     // The tree associated with this FMM, just has to
    implement Tree trait, can be single or multi-node.
7     pub tree: T,
8
9     // The kernel associated with this FMM.
10    pub kernel: U,
11
12    // The M2L operator associated with this FMM, can be
    specialised to be sparsified using different methods.
13    pub m2l: V,
14 }
15
16 pub struct KiFmmData<T: Fmm> {
17     // A field holding our FMM algorithm
18     pub fmm: T,
19
20     // Data fields, shown as placeholders
21     pub multipoles: ...,
22     pub locals: ...,
23     pub potentials: ...,
24     pub points: ...,
25     pub charges: ...,
26 }

```

Listing 2.3: Structs that specify a concrete implementation of an FMM algorithm.

By implementing the traits for the translation operators in Listing 2.4 for the struct corresponding to our algorithm’s data (e.g. `KiFmmData`), and the FMM loop structure for the algorithm type (`KiFMM`), we can now re-implement new FMM algorithms by changing the structs in Listing 2.3 and Listing 2.2. This highly flexible approach allows a user to directly compare the relative differences between two variables in an FMM implementation while keeping other features, such as the underlying tree, or kernel being evaluated, constant. Indeed this is how we implement an SVD and FFT T^{M2L} operator for the `kiFMM`, which are contrasted in Section 3.2.2. This amounts to an implementation of the FMM following the open/close principle as Rust traits can also be implemented by downstream users of a crate. For example, if a user wanted to rewrite the `Kernel` to use a different hardware such as a GPU, they would simply have to implement the corresponding trait methods for their GPU based kernel, and pass this to the `kiFMM` struct, making our software readily extensible.

```

1 pub trait SourceTranslation {
2
3     // Particle to multipole translation.
4     fn p2m(&self);
5
6     // Multipole to multipole translation.
7     fn m2m(&self, level: u64);
8 }

```



```

9
10 pub trait TargetTranslation {
11     // Local to local translation.
12     fn l2l(&self, level: u64);
13
14     // Multipole to particle translation.
15     fn m2p(&self);
16
17     // Particle to local translation.
18     fn p2l(&self);
19
20     // Local to particle translation.
21     fn l2p(&self);
22
23     // Near field interactions.
24     fn p2p(&self);
25 }
26
27
28 pub trait FmmLoop {
29
30     // Compute the upward pass.
31     fn upward_pass(&self, time: Option<bool>) -> Option<
TimeDict>;
32
33     // Compute the downward pass
34     fn downward_pass(&self, time: Option<bool>) -> Option<
TimeDict>;
35
36     // Compute the upward and downward passes
37     fn run(&self, time: Option<bool>) -> Option<TimeDict>;
38 }

```

Listing 2.4: Traits that are implemented over FMM Data structs, and FMM algorithm structs

Of course one could replicate similar functionality in an object oriented language, by similarly defining methods over structs, however in Rust we benefit from the fact that contracts specified by Traits are checked by the compiler as a part of the type system. Thus strictly enforcing the behaviour that we expect, even for downstream users of Traits. For example, when implementing the FmmLoop trait in Listing 2.4 we do not know about the specifics of how the kernels, trees, or T^{M2L} have been implemented. This is an example of Rust's Traits allowing us to write code with dependency inversion built-in.

Open Work Streams

3.1 Distributed Octrees

In this section we describe our software for the creation of octrees for the kiFMM in \mathbb{R}^3 , Bempp-Tree¹. We’ve re-implemented optimal algorithms for the ‘bottom-up’ construction of trees in parallel, whereby points distributed across each node are assembled into a parallel tree partitioned and load-balanced across a distributed system [37]. We demonstrate that on a single-node, our tree software performs well in comparison to leading single-node FMM codes [43], where parallel experiments are omitted due to time constraints. In addition to good scaling, we leverage the power of Rust’s Traits to write software that generalises across single-node and multi-node trees, allowing for users to implement single/multi-node fast algorithms with relative ease. We begin by describing in detail our method for constructing trees, following the discussion in [37] though we use an updated communication scheme in order to achieve a 2:1 balance based on more recent work in [36]. We conclude with a short discussion on the communication intensive phases of the FMM in a distributed-memory FMM implementation, and how these can be addressed, as the next stage of this research project centers on the construction of a distributed memory kiFMM.

We make use of a standard space-filling curve known as a Morton encoding [37] to encode the boxes of an octree as described in Figure 3.1. This approach encodes spatial locality in that boxes encoded in sorted Morton order correspond to a pre-order traversal of the corresponding octree. Once encoded the Morton encoding for a given box is referred to as a *Morton key*. The main terminology which we will make use of with regards to trees created using Morton encodings are summarised Table 3.1.

Historically implementations of distributed memory octrees and quadrees were ‘pointer based’ [40]. Starting with a random subset of points at each processor, each node would recursively refine its local octree until it arrived at level of recursion limited by a user defined constraint on the maximum number of particles in a leaf box. However this is complicated by the need to communicate and synchronise ancestor relationships across nodes. Furthermore as the point distribution is not generally known apriori, with each process controlling a local tree involving a subset of the initial points, reconciling local trees necessitates a global parallel merge. Overlapping boxes would result in the user defined constraint on the maximum number of particles per box being violated, necessitating further refinement. Further communication would then be required if a user requires a 2:1 balance. Finally, load-balancing to ensure each node has an approximately uniform weighting in terms of particles would be computed as a post processing step.

The significant complexities in implementing such trees has lead to softwares that

¹<https://github.com/bempp/bempp-rs/tree/main/tree>

rely on a ‘bottom up’ approach, as opposed to a ‘top down’ strategy as described above [30, 8]. The basic strategies implemented here is to form a Morton encoding for points at each processor and use parallel sorts to ensure that each node contains a non-overlapping subset of the global tree. The Morton keys are kept only at the leaf level, with ancestor keys inferred to exist. These trees are therefore referred to as *linear* trees, and have been shown to scale to trees created of tens of thousands of processors with billions of octants [8].

Beginning with point data distributed across n_p nodes in a distributed memory system, our strategy for creating uniform and adaptive octrees is as follows,

1. Generate a Morton key for each point at the leaf level corresponding to a user defined octree depth (uniform trees), or based on a critical value for the maximum number of points per leaf box (adaptive trees).
2. Perform a parallel sort of these leaf octants, such that processors contain non-overlapping subsets of the global tree.
3. *Linearise* the leaves on each compute node, i.e. remove overlaps, favouring smaller leaves over larger ones. We use Algorithm 4 in Appendix E to do so.
4. ‘Complete’ the space defined by the largest and smallest leaf on each compute node. This amounts to finding the minimal octree that covers the region specified by the Morton keys at each process. This is described by Algorithm 5 in Appendix E. The coarsest boxes of this ‘complete’ tree are referred to as ‘seeds’.
5. Construct a ‘coarse block tree’ by completing the space between seeds on each processor. The nodes of this tree are referred to as blocks, and help us to estimate the load balance of each compute node by calculating the number of original Morton keys they contain. This gives us a coarse distributed, complete, linear octree that is based on the underlying data distribution and contains load information.
6. Point data is communicated to each compute nodes containing its associated block, and the blocks are refined based on the level of recursion defined by the user, which depends again on whether uniform or adaptive trees are required. Providing the final, unbalanced, tree in the case of adaptive trees.
7. For adaptive trees a 2:1 balance is computed on each subtree on each compute node using Algorithm 6 in Appendix E. The locally balanced leaf octants can be sorted in parallel again, and locally linearised as in Step 3, to remove overlaps. Thus we are left with a globally balanced, linear, octree based on the original data distribution.

This algorithm is summarised in Algorithm 7 in Appendix E. The complexity of this process is bounded by the parallel sorts, which for randomly distributed point data, run in $O(N_{\text{leaf}} \log(N_{\text{leaf}}))$ work and $O(\frac{N_{\text{leaf}}}{n_p} \log(\frac{N_{\text{leaf}}}{n_p}) + n_p \log(n_p))$ time where N_{leaf} is the number of leaves in the final octree, and n_p is the number of MPI processes [36]. This makes the efficiency of the parallel sort a bottleneck in tree construction.

Designing and implementing an efficient sorting algorithm that can scale to thousands of cores is difficult since it requires irregular data access, communication, and

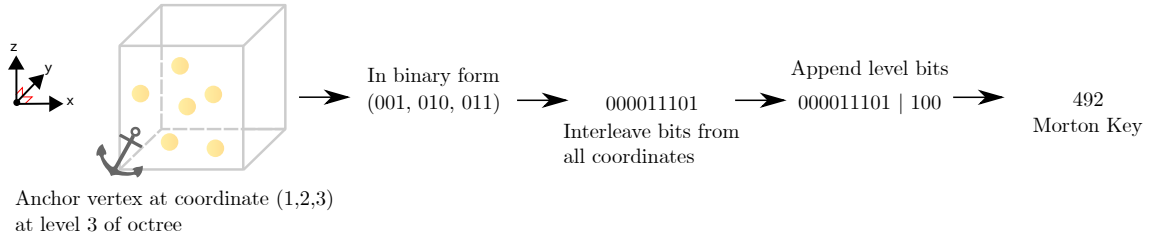


Figure 3.1: How to Morton encode a node in an octree. The node is described by an ‘anchor’ vertex, and its associated coordinate.

Relation	Definition
$\text{Siblings}(N)$	The seven (octree) or three (quadtrees) Keys that share a parent with N
$\text{Neighbours}(N)$	Keys that share a face, edge, or vertex with N
$\text{Parent}(N)$	The parent key of N
$\text{Children}(N)$	The eight (octree) or four (quadtrees) children of N
$\text{Descendants}(N)$	All descendants of N
$\text{Ancestors}(N)$	All ancestors of N
$\text{FinestAncestors}(N, M)$	Finest shared ancestor of N and M .
$\text{FirstChild}(N)$	The ‘first’, in Morton order, child of N
$\text{LastChild}(N)$	The ‘last’, in Morton order, child of N
$\text{DeepestFirstDescendant}(N)$	The ‘first’, in Morton order, descendant of N at the leaf level
$\text{DeepestLastDescendant}(N)$	The ‘last’, in Morton order, descendant of N at the leaf level

Table 3.1: Definitions of Morton key relations for a given Morton key N .

equal load-balance. As first presented by Sundar et al, parallel sorts in the creation of octrees were implemented using a variant of Sample Sort [37]. Briefly, this approach samples elements at each processor to create a set of $n_p - 1$ ordered ‘splitters’, which are shared across all processors and define a set of n_p buckets. This is followed by a global all-to-all communication call over all n_p processors to assign elements to their corresponding bucket. Finally, a local sort is performed at each bucket to produce a globally sorted array. SampleSort is well understood. However, its performance is quite sensitive to the selection of splitters, which can result in load imbalance. Most importantly, the all-to-all key redistribution scales linearly with the number of tasks and can congest the network. As a result sample sort may scale sub-optimally, especially when the communication volume approaches the available hardware limits [36].

An alternative approach is provided by HykSort [36], which is a generalisation of Quicksort over a hypercube [42] from 2-way splits to k -way splits, with the addition of an optimised algorithm to select splitters. Quicksort, Hyksort and Sample Sort are compared in figure (3.2). Instead of splitting the global array into n_p buckets, Hyksort splits it into $k < n_p$, and recursively sorts for each bucket. We notice that at each recursion step, each task communicates with just k other tasks. Indeed, for $k = 2$ we recover Quicksort over a hypercube. Both Hyksort, and the parallel splitter selection algorithm are provided in Appendix B, alongside complexity comparisons between Hyksort and Sample Sort. We note that Hyksort has a lower asymptotic complexity, with no terms that scale linearly in number of MPI processes, n_p , unlike

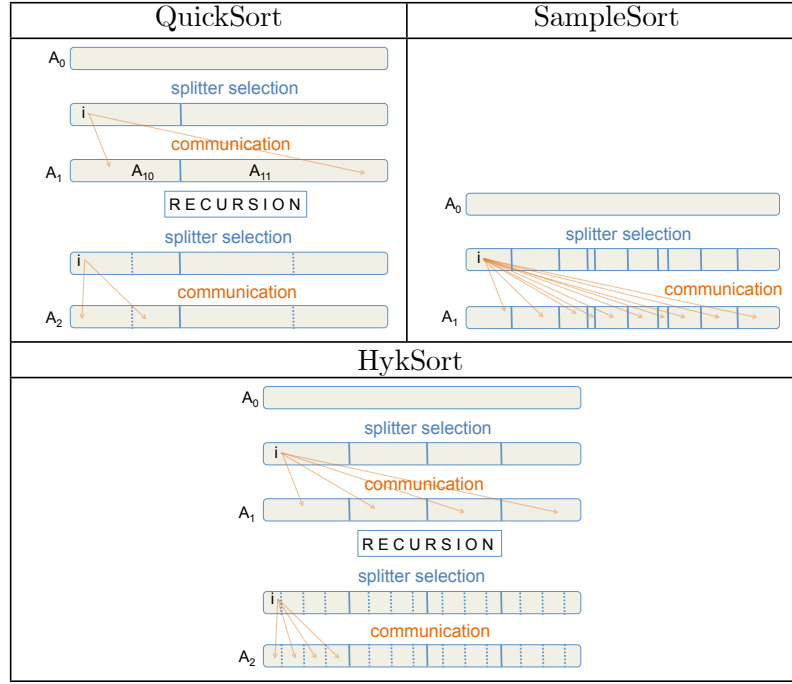


Figure 3.2: Communication pattern of Hyksort algorithm compared to a parallel Sample Sort, as well as a Quicksort over a hypercube, adapted from [36]. We see that HykSort results in a lower communication overhead than Sample Sort.

Sample Sort.

Figure 3.3 shows scaling of our software, ‘Bempp-Tree’, on a single node as time limitations inhibited multi-node experiments. In the left figure compare the performance of linear trees constructed using our software with the pointer-based trees constructed using the functionality of ExaFMM-t the leading single-node implementation of the kiFMM. We limit this comparison to uniform trees as they don’t offer adaptive functionality. In the right figure we show weak scaling for fixed $1e6$ points per MPI process for adaptive and uniform trees. We observe that there is a constant overhead in constructing adaptive trees, this comes from having to recursively refine blocks from the block tree by counting how many points they contain. The significant jump when using 8 MPI processes is likely due to the number of MPI processes exceeding the number of cores available on the Intel i7-9750 processor used for the experiments. Our performance in the single-node case is excellent, where we’re able to generate an octree with $8e6$ points, with a depth of 5, in approximately 13.5s. A marked improvement over ExaFMM-T, and demonstrative of the power of a bottom up approach in comparison to a pointer based approach used by that software. Multi-node experiments are required to assess the performance of our library in comparison to other state of the art tree libraries [30, 8]. However, as our approach closely follows theirs we don’t expect performance to be significantly different.

3.1.1 Exposing Parallelism in A Distributed Memory FMM

In the context of FMMs generating a distributed tree constitutes the first communication intensive phase. Further bottlenecks occur in the evaluation of the operators, most significantly in the evaluation of T^{M2M} and T^{M2L} . To understand where these operators lead to communication bottlenecks, and how these can be overcome in practical implementations, we now introduce terminology relevant to distributing the FMM on parallel machines. We build upon the discussion first presented in

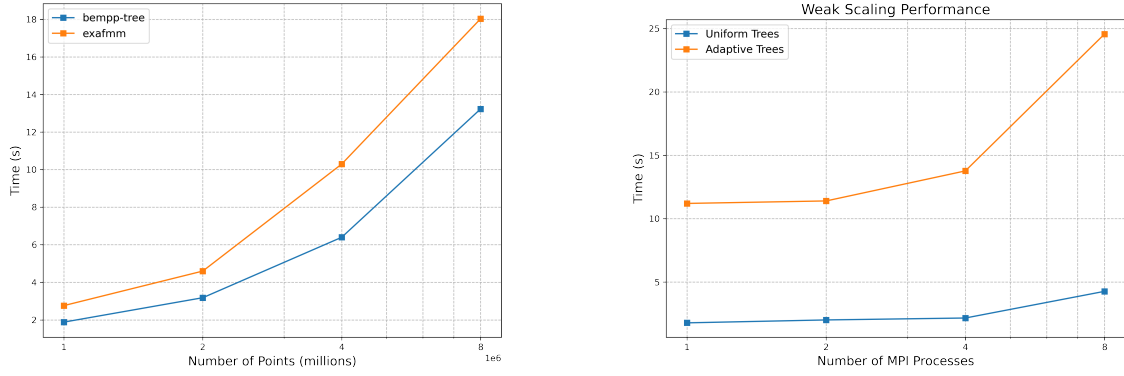


Figure 3.3: The left figure shows the runtime of creating uniform trees on a single node in Bempp-Tree, in comparison to ExaFMM-T. The right figure shows weak scaling (over cores on a single node) of creating uniform and adaptive trees with Bempp-Tree, where each MPI process is given $1e6$ points. The uniform trees are partitioned to a depth of 5, the adaptive trees have at most 150 particles in their leaf boxes. Experiments were taken on an Intel i7-9750H 6 core processor.

Section 3 of [22], and use the same terminology.

Given a partition of a global tree T , as described above, such that each compute node k contains a disjoint subset of leaves arranged in morton order, T_k we define a *Locally Essential Tree* (LET) for compute node k as the union of interaction lists for all its owned leaves, as well as their ancestors,

$$\text{LET}(k) := \cup_{N \in T_k \cup \text{Ancestors}(T_k)} \text{InteractionList}(N) \quad (3.1)$$

We denote the region controlled by MPI process k as Ω_k , from the properties of Morton keys (see app. E) this is defined by the smallest and largest Morton key they hold. Using an MPI_AllGather collective, we exchange information about the bounds of each MPI process globally. Following this, ancestors are added to each T_k for the leaf nodes they control. In order to communicate ‘ghost octants’, i.e. octants which are relied upon by the translation operators acting upon each T_k but are not held locally, we introduce the concept of ‘Contributor’ and ‘User’ compute nodes,

1. Contributor compute nodes for an octant $N \in T$ are

$$\mathcal{P}_c(N) := k \in 1..p : N \text{ overlaps with } \Omega_k$$

2. User compute nodes of an octant $N \in T$ are

$$\mathcal{P}_u(N) := k \in 1..p : \text{Parent}(N) \text{ or Neighbours}(N) \text{ overlaps with } \Omega_k$$

We denote the set of octants which compute node k contributes and which process k' uses as $I_{kk'}$. These are communicated and inserted into each compute node’s local tree in order to complete the construction of its LET. Consider the potential generated by the sources enclosed by some octant N . In order to evaluate the potential outside the volume covered by $\text{Neighbours}(\text{Parent})(N)$ one doesn’t need the multipole expansions, or sources, associated with N as an ancestor of N would be used instead. This ensures the correctness of this approach to constructing LETs.

Once an LET has been constructed, and particle information has been exchanged to user processors, the T^{P2M} and $P2P$ operators don't require further communication. Lashuk et. al reason that this allows for the potential pipelining of T^{P2M} , T^{M2M} and T^{M2L} , though they have not experimented with this. They identify the T^{M2M} and T^{M2L} operators as those requiring intensive communication phases during FMM evaluation. Beginning with T^{M2M} , the communication and calculation can be seen to progress in three steps,

1. Firstly, source charges which are required for $P2P$ are communicated with user MPI processes. As these will be relatively 'local' communications within the context of a distributed memory machine, they use non-blocking point-to-point 'Isend' functions for this step.
2. Secondly, the multipole coefficients are summed for the octants on the coarser level.
3. Thirdly, the multipole coefficients are communicated to user octants, as each MPI rank has only a partial sum for the octants at the parent level of each octant.

During the downward pass Lashuk et. al.'s scheme doesn't require any further communication as each MPI process has all the multipole data, as well as point data, to compute the FMM for its locally held particles in parallel. The complexity of the communication of this scheme is given as $O(\sqrt{n_p}(N/n_p)^{2/3})$ where n_p is the total number of MPI processes and N is the number of particles for octrees created in \mathbb{R}^3 . This complexity applies as upper bound for non-uniform point distributions.

Ibeid et. al [18] propose an alternative communication scheme that achieves a tighter complexity bound of $O(\log(n_p) + (N/n_p)^{2/3})$. They rely on an alternative abstraction for handling the tree, by splitting it into a 'global tree' and 'local tree'. Their scheme is illustrated in Figure 3.4, which describes a uniformly refined tree created for uniform point distributions², which we've adapted from Figure 3 in [18]. Here a global tree is constructed such that the *root node* of the tree on each MPI process is *leaf node* of the global tree. The depth of the global tree, defined by L_{global} in fig 3.4, is thus defined by the number of MPI processes and is therefore $O(\log(n_p))$. The depth of the local tree is defined by the particles belonging to the MPI process and is seen to be $O(\log(N/n_p))$. By splitting the tree in this way, the communications during the T^{M2M} and T^{M2L} operators can be split into 'global' and 'local' phases. At the leaf nodes of the global tree, which starts at level L_{global} , after T^{M2M} is performed, 8 neighbouring MPI processes contain the same information for boxes at $L_{\text{global}} - 1$. Therefore, only one of them has to perform communications for the T^{M2M} operation for the next level, proceeding recursively until the root of the global tree is reached. This corresponds to an 8-fold redundancy in the communication scheme proposed by Lashuk et. al. Using this, the number of communications at coarser global tree levels for each box stays constant at 7, and the communication complexity of the T^{M2M} operator is proportional to the depth of the global tree $O(\log(n_p))$. The same redundancy can be used in reverse during the downward pass to communicate the multipole coefficients during T^{M2L} on the global tree, which has the same complexity. We note however that in practice communications will occur between increasingly distant nodes at coarser levels of

²This is proved for uniform point distributions, and a uniformly refined octree in [18], but is also demonstrated to apply to non-uniform distributions.

the tree, meaning that specific network topologies or interconnects would have an impact on practical performance.

Communications are still required during the downward pass of the local trees for computing T^{M2L} and the $P2P$ operators. However, the communications are ‘local’ in the sense that the same set of MPI processes will communicate with each other due to their overlapping LETs. This limits the number of processes to communicate with to $O(1)$ during these steps, as opposed to $O(n_p)$. However, as the number of boxes increases exponentially at finer tree levels, the amount of information being sent grows with increasing tree depth. This amounts to an increasing ration of the surface to volume for finer boxes. The same is true for communicating the source point data for the $P2P$ operator. They find the number of boxes to be sent for T^{M2L} at the i^{th} level of the local tree to be $(2^i + 4)^3 - 8^i$ and $(2^i + 2)^3 - 8^i$ respectively. This can be seen by the fact that the interaction list for T^{M2L} requires the communication of a halo that is 2 boxes wide, which adds 4 boxes per dimension, and similarly the $P2P$ requires the communication of a halo that is 1 box wide, which adds 2 boxes per dimension, and there are 8^i boxes at the i^{th} level. Summing up the powers of four up to the depth of the local tree gives,

$$\sum_i^{\log_8(N/n_p)} 4^i = (N/n_p)^{\log(4)/\log(8)} = (N/n_p)^{2/3} \quad (3.2)$$

Giving a communication complexity of $O((N/n_p)^{2/3})$ for the local tree communications, and proving the bound provided by Ibeid et. al.

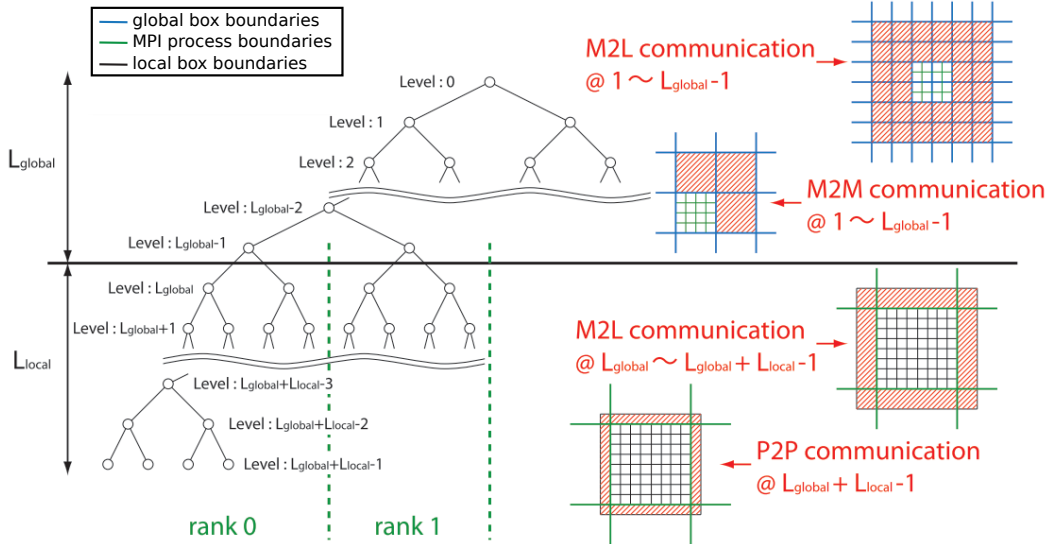


Figure 3.4: The tree structure shown here is a binary tree chosen for clarity by Ibeid et. al, this would be an octree in \mathbb{R}^3 .

The near term priorities for our tree implementations are to implement the optimised communication scheme of Ibeid et. al., and compare its practical performance with the scheme provided by Lashuk et. al. Real architectures may offer discrepancies in performance from the that expected from complexity analysis as Ibeid et. al’s approach results in communication between physically distant MPI processes

and the scheme of Lashuk et. al. benefits from being simpler to implement, with low-effort opportunities for further optimisations through operation pipelining and has been demonstrated to scale well to thousands of MPI processes, with billions of points.

3.2 Fast Field Translations

As noted in Chapter 2.3, the T^{M2L} is the most computationally intensive phase of an FMM implementation. In this section we describe two major approaches to accelerate its computation, chiefly a numerical compression scheme based on taking an SVD and relying on the low-rank nature of T^{M2L} , and secondly an ‘exact’ method that relies on an FFT to reduce the complexity of the convolution represented by T^{M2L} . We have implemented both via our software ‘Bempp-Field’³, and we use this section to describe the relative merits of these approaches, implementation challenges, as well as open questions which remain. We find that the FFT approach, which has been demonstrated to perform well in single node [43] as well as multi node [25] settings to be our favoured approach. We propose new algorithm for its implementation, and offer some benchmarks for its performance in a single-node setting relative to the state of the art [43, 25] which rely on a similar approach.

3.2.1 SVD Field Translations

In order to uniquely label M2L interactions we introduce transfer vectors $t = (t_1, t_2, t_3)$, $t \in \mathbb{Z}^3$. They describe the relative positioning of two boxes, X and Y , in a hierarchical tree and are computed from their centres $t = \frac{c_x - c_y}{w}$ where w is the box width.

Consider the application of T^{M2L} , to a given multipole expansion q , where our goal is to compute the check potential ϕ ,

$$\phi = T^{M2L} q \quad (3.3)$$

As T^{M2L} is known to be low-rank, it can be optimally approximated with an SVD,

$$\tilde{\phi} = U_k \Sigma_k V_k^T q \quad (3.4)$$

where k indicates the rank of T^{M2L} , i.e. the smallest non-zero singular value. This can be shown to be an optimal approximation to K [39]. For homogenous, translationally invariant kernels we see from Table 2.1 that there are at most 316 unique translation vectors corresponding to T^{M2L} operations in \mathbb{R}^3 . Stacking their corresponding discrete matrices column wise,

$$T_{\text{fat}}^{M2L} = [T_1^{M2L}, \dots, T_{316}^{M2L}] \quad (3.5)$$

$$= U \Sigma [V_1^T, \dots, V_{316}^T] \quad (3.6)$$

or row-wise,

³<https://github.com/bempp/bempp-rs/tree/main/field>

$$T_{\text{thin}}^{M2L} = [T_1^{M2L}, \dots, T_{316}^{M2L}] \quad (3.7)$$

$$= [R_1^T; \dots; R_{316}^T] \Lambda S^T \quad (3.8)$$

we note that,

$$T_{\text{thin}}^{M2L} = (T_{\text{fat}}^{M2L})^T \quad (3.9)$$

for such kernels which are symmetric. Having computed these two SVDs we can reduce the application cost of a given T_i^{M2L} between two boxes,

$$T_i^{M2L} q = R_i \Lambda S^T q \quad (3.10)$$

Using the fact that S is unitary, i.e. $S^T S = I$, we can insert this into equation (3.10) to find,

$$T_i^{M2L} q = R^{(i)} \Lambda S S^T S^T q \quad (3.11)$$

$$= T_i^{M2L} S S^T q \quad (3.12)$$

$$= U \Sigma V_i^T S S^T q \quad (3.13)$$

$$(3.14)$$

Now using that U is also unitary such that $U^T U = I$, we find

$$T_i^{M2L} q = U U^T U \Sigma V_i^T S S^T q \quad (3.15)$$

$$= U [U^T U \Sigma V_i^T S] S^T q \quad (3.16)$$

$$= U [U^T T_i^{M2L} S] S^T q \quad (3.17)$$

The bracketed terms can be calculated using the rank k approximation from the SVD,

$$[U^T T_i^{M2L} S] = \Sigma V_i^T S \quad (3.18)$$

$$= U^T R_i \Lambda \quad (3.19)$$

We call equation (3.19) the *compressed T^{M2L} operator*.

$$C_i^k = U^T T_i^{M2L} S \quad (3.20)$$

This matrix can be precomputed for each unique interaction. Therefore in the kernels considered in this exposition, it must be computed at most 316 times, with corresponding pre-computations for kernels with different properties.

The application of T^{M2L} can now be broken down into four steps.

1. Find the ‘compressed multipole expansion’

$$q_c = S^T q$$

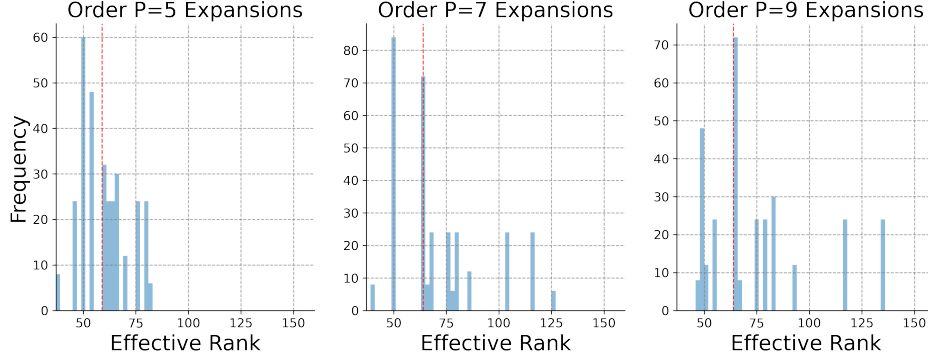


Figure 3.5: Rank behaviour of T^{M2L} computed for the Laplace kernel at different expansion orders presented as a distribution over the 316 unique transfer vectors for this kernel. We estimated the ranks of each matrix by counting the number of singular values greater than 10^{-10} . The red dashed line indicates a median rank, for $P = 5$ it was found to be 59. for $P = 7$ and 9 it was found to be 64.

2. Compute the ‘compressed check potential’, where the sum is taken over all boxes which have an applicable T^{M2L} operator, ie its interaction list.

$$\phi_c = \sum C_i^k q_c$$

3. Post process to recover an uncompressed check potential

$$\phi = U\phi_c$$

4. Finally, calculate the local expansion from the check potential as done previously in Section 2.3.

The rank behaviour of T^{M2L} has been assumed to be low-rank throughout this thesis, and therefore amenable to compression. However it remains an open question as to the exact rank behaviour of a given kernel in practice. This has consequences for real implementations, as if we are able to effectively cut-off the rank k with $\kappa \ll k$ we may be able to reduce the complexity of the SVD based scheme T^{M2L} further. Figure 3.5 shows the effective rank behaviour of the Laplace kernel for different expansion orders. In this experiment we calculated the number of singular values greater than a threshold of 10^{-10} for all 316 unique transfer vectors for the Laplace kernel. We see that that width of the distribution has a strong relationship with the expansion order P , however the median rank remains approximately the same regardless of the expansion order. This implies that there is some dependency of the low-rank approximation for smaller transfer vectors for larger expansion orders. Analytical investigations could reveal what this is explicitly, as this would inform the cut-off value taken for κ , as it is an open question to what this behaviour is explicitly. Understanding this would inform practical implementations of an SVD based approach to sparsifying T^{M2L} .

Practical implementations can re-formulate the SVD based scheme to increase the computational intensity⁴ of the operation. As presented above, each box B will have to compute T^{M2L} for each box in its relevant interaction list, up to 189

⁴The computational intensity is short hand for the ratio of computations to memory accesses, i.e. flops/bytes.

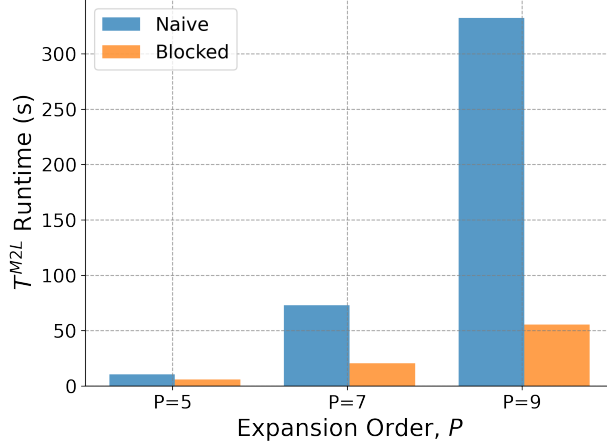


Figure 3.6: Here we illustrate two schemes for computing T^{M2L} in Rusty Field. The ‘Naive’ scheme performs a parallel loop over the boxes at each level, looks up their associated T^{M2L} and computes check potentials as a matrix-vector product. The blocking scheme uses the re-organisation outlined above to block together T^{M2L} s corresponding for all source/target boxes at a given level with matching transfer vectors, and thus computing a matrix-matrix product. Here we don’t choose a cutoff rank κ , and all T^{M2L} matrices are left uncompressed. Experiments are taken on a 6 core Intel i7-9750 processor using Open BLAS, we report maximum runtimes over 5 runs for each set of parameters.

times in \mathbb{R}^3 . For each of these applications, B will have to look up the appropriate compressed T^{M2L} from memory in this naive scheme. Matrix vector products are handled by BLAS level 2 operations, however by taking advantage of BLAS level 3 operations we can increase the ratio of computations to memory accesses. We do so in our implementation by blocking together *all* the right hand sides, i.e. multipole expansions, which share a given translation vector t and compute their compressed check potentials in a single matrix-matrix product. This has a dramatic effect on the runtime of our software as shown in Figure 3.6.

We note that the precomputation for this approach relies on an SVD of two relatively large matrices in (3.6) and (3.8) where we use the ‘greedy’ DGESVD provided by LAPACK. For the Laplace kernel, which is translationally invariant and homogenous, precomputation times are shown in Figure 3.7. However, for kernels which are translationally invariant but not homogenous, these must be computed for each level of the octree which can have a significant impact on setup time for the FMM, dominating the tree setup time as well as the algorithm runtime. This could be alleviated with alternative implementations that make use of randomised algorithms, which have been shown to have considerably faster runtimes for a given compression rank [16], though we haven’t explored this as of date.

3.2.2 FFT Field Translations

From the structure of our kernels of interest (2.2), as well as the fact that our equivalent densities and check potentials are arranged on a regular grid (fig. 2.4), we notice that the calculation of the downward check potential during T^{M2L} is a convolution,

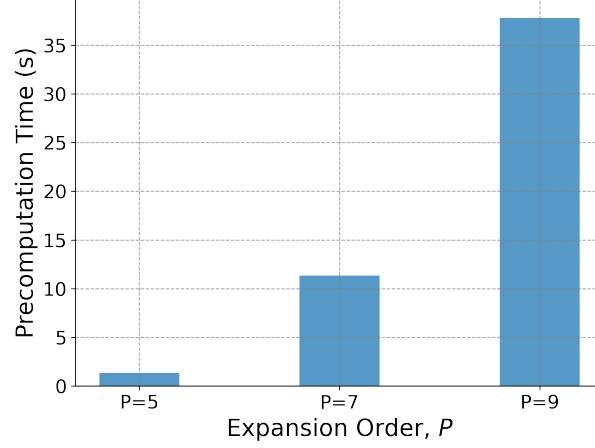


Figure 3.7: Here we illustrate the precomputation time to compute the SVDs of T^{M2L} for a selection of expansion orders. We observe that precomputation time can grow dramatically with increased expansion order, for $P = 9$ precomputation rivals the runtime of T^{M2L} (see fig. 3.6). Experiments are taken on a 6 core Intel i7-9750 processor using Open BLAS, we report maximum runtimes over 5 runs for each set of parameters.

$$\phi = (K * q)(x) = \int_{y^{B,d}} K(x - y) q^{A,u}(y) dy \quad (3.21)$$

When translating the multipole expansion at a box A to a box B . From Fourier theory, the property of the Fourier transforms of a convolution is that they are the product of two individual transforms,

$$\mathcal{F}\{K * q\}(k) = \mathcal{F}\{K\}(k) \cdot \mathcal{F}\{q\}(k) \quad (3.22)$$

where k denotes the frequencies in Fourier space. We therefore find that the check potential can be computed as,

$$\phi(x) = \mathcal{F}^{-1}\{\mathcal{F}\{K\}(k) \cdot \mathcal{F}\{q\}(k)\}(x) \quad (3.23)$$

In practice for the kiFMM the sequence corresponding to K must contain all the unique evaluations of the kernel (2.2) between a source box A and a target box B . This sequence is constructed with the help of an ancillary data structure known as a ‘convolution grid’.

We illustrate the construction of the sequences that are required for an FFT based T^{M2L} in \mathbb{R}^2 , however they are directly applicable to \mathbb{R}^3 . Consider Figure 3.8, which shows a source and target box, each of which is annotated with source equivalent points y_i and target check points, x_i , for a $P = 2$ expansion.

The equivalent surface around the source box is *embedded* within a convolution grid, as shown in Figure 3.9, such that the number of points on a convolution grid is P^3 in \mathbb{R}^3 and P^2 in \mathbb{R}^2 respectively.

The unique kernel interactions between the source equivalent surface and the target check surface in (3.21) are computed with respect to a single point on the

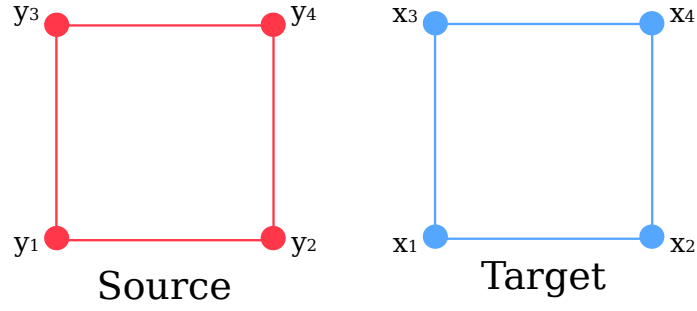


Figure 3.8: A source and target box, with source and target locations on the respective equivalent and check surface annotated..

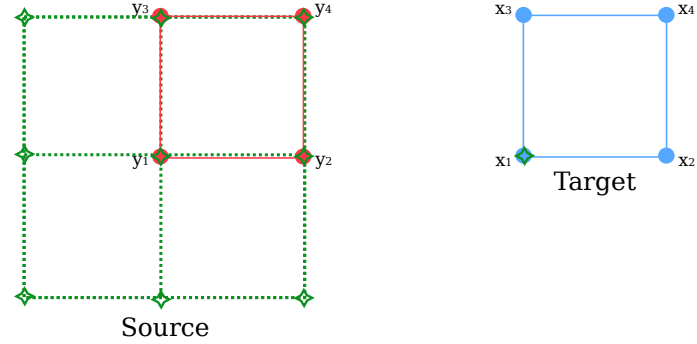


Figure 3.9: The source equivalent surface is embedded within a (green) convolution grid. The points on the convolution grid are marked with diamonds. An additional diamond is placed on the target check surface, which identifies the point with which kernels are evaluated with respect to.

target check surface and the points on the convolution grid. We then see that we must compute the convolution of two sequences in \mathbb{R}^2 , illustrated in Figure 3.10. Here the first sequence is the unique kernel evaluations taken with respect to a fixed point on the target check surface, and the second sequence is the multipole expansion coefficients mapped to the convolution grid from the source box's equivalent surface. We proceed to take Fourier transforms via the FFT for both of these sequences, and compute their convolution via a Hadamard product.

Computing this Hadamard product, for which we use the FFT, results in another sequence illustrated in Figure 3.11, where we have taken care to ‘flip’ the sequence corresponding the unique kernel evaluations as required by the definition of a convolution. We find the final check potentials by taking the inverse Fourier transform

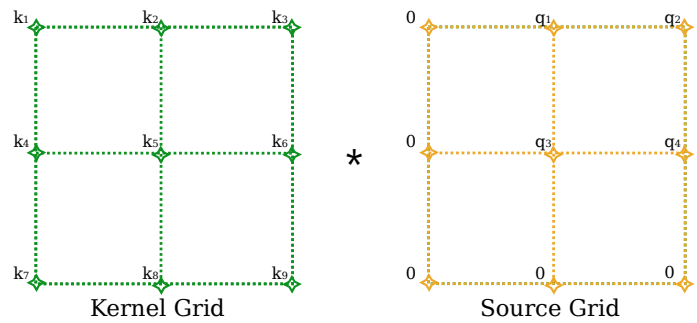


Figure 3.10: A Hadamard product is computed between the Fourier transforms sequence of unique kernel evaluations and the multipole expansion coefficients which are also placed on the convolution grid.

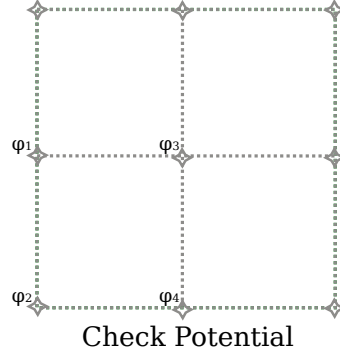


Figure 3.11: The result of the convolution illustrated in Figure 3.10, on the convolution grid. We only identify locations that correspond to check potentials, as the other entries will contain results which are not required, corresponding to redundant computations with this method.

of it.

We note that although we rely on the existence of a convolution grid to compute the required sequences, in practice we do not compute or store it. We simply require a mapping between the index locations of points on the equivalent surfaces to their corresponding positions on a convolution grid.

Expressed alternatively, we can represent the points on an equivalent surface, $y \in y^{B,u}$, by their respective indices $y_{i,j,k}$ when in \mathbb{R}^3 . The elements corresponding to the unique kernel interactions are then,

$$K_{ijk} = K(x_{000} - y_{ijk}) \quad (3.24)$$

where x_{000} is the index of a point on the target equivalent surface with which the sequence is calculated with respect to. We choose the bottom left corner on the target surface, though in principle any point could be used, it would just amount to a translation of the convolution grid. This results in a 3D sequence $K[\cdot]$, with elements,

$$K[i, j, k] = K_{i,j,k} \quad (3.25)$$

Again the symmetries of kernels make the Fourier transforms of this quantity something that has the potential to be pre-computed and cached, in a similar way to which the SVD based T^{M2L} could be cached. At runtime, we simply need to look up the corresponding sequence $\hat{K}_t[\cdot]$ corresponding to a transfer vector t between a given source and target box, and compute the convolution as outlined above. The reduced complexity of the FFT in comparison to an SVD results in greatly faster pre-computation times (see fig. 3.14 as opposed to fig. 3.7).

The Hadamard product has a low computational intensity⁵, and naive implementations can be slow in practice regardless of the superior complexity of the FFT based T^{M2L} in comparison to the compressed matrix vector products of the SVD approach outlined in the previous section especially when combined with optimisations to use BLAS3 operations. The authors of the leading multi-node bbFMM [25] use a strategy of considering sets of siblings together, alongside explicit SIMD to increase the computational intensity of this operation. This approach is re-implemented by

⁵Ratio of flops to memory accesses.

the authors of the leading single-node kiFMM [43], though involves computes redundant T^{M2L} translations. We explain briefly how this works below, before introducing our own approach which though similar, avoids these redundancies.

Consider a source box alongside its siblings in \mathbb{R}^3 ,

$$S = \cup_{i=1}^{N=8} S_i \quad (3.26)$$

For each unique T^{M2L} we have a sequence $K[]$, and can pre-compute a sequence $\hat{K}[]$ corresponding to their Fourier transforms. Considering the sibling set S 's parent box, we can compute T^{M2L} with respect to the neighbours of S 's parent. This results in $64 = 8 \times 8$ for translations between S and the children in a particular neighbour of their parent, with corresponding sequences $\hat{K}[]$. We note that not all of these translations are necessarily required, the authors of [25, 43] simply take the convolutions with respect to zero data used for the corresponding multipole expansion. When repeated for all of the neighbour's of S 's parent, we're left with a total of $1664 = 8 \times 8 \times 26$ applications of T^{M2L} for a given sibling set S . Despite containing redundant calculations, the implementation is highly cache-optimised. The authors of [25] proceed by iterating over each of S 's parent's neighbours - pulling out the i^{th} frequency component from each - leading to a sequence of length $8 \times 8 \times 26$, they proceed by pulling out the i^{th} frequency component of the Fourier transform of each sibling - leading to a sequence of length 8. The Hadamard product is found by computing 26 individual 8×8 operation using explicit SIMD. By iterating over S 's parent's neighbours in the outer loop the sequence of length $8 \times 8 \times 26$ can be held in memory for each subsequent sibling set.

This strategy is known to perform well. An experiment with the Laplace kernel, order $P = 9$ expansions, and 1e6 source/target points takes at most 2.7s to evaluate T^{M2L} on a 6 core Intel i7-9750H processor⁶. However, we note that the redundant computations can be reduced.

We begin by noting that for our kernels of interest correspond lead to 316 unique translation vectors t with corresponding T^{M2L} operators, however the majority of these operators correspond to reflections of each other. First introduced by Messner et. al [28] in the context of an SVD based acceleration of T^{M2L} , where they attempt to reduce the size of the SVD required for the pre-computation in this approach, one can reduce the number of transfer vectors corresponding to *unique* T^{M2L} to just 16. In the original paper they aimed to demonstrate that with just 16 unique T^{M2L} BLAS3 matrix-matrix products would further reduce the application time of the compressed T^{M2L} operator, however as we demonstrate in Figure 3.12, we don't observe this to have a significant effect on the runtime of the matrix-matrix products of the sizes expected in a typical FMM, at least on modern processors as used during testing.

In order to see how we arrive at 16 unique T^{M2L} operators we introduce two symmetries, building upon the discussion in [28]. They describe two planes of symmetry, axial and diagonal, when considering a source box A and a target box B during a given interaction specified by a T^{M2L} operator. This is sketched for \mathbb{R}^2 for clarity in Figure 3.13, where we show three sources A with their respective transfer vectors, t , with respect to B . These boxes describe the equivalent/check surfaces described above for the kiFMM and the quadrature points are labelled by an index coordinate for an expansion of $P = 2$. The axial planes of symmetry are given by

⁶Experiments were repeated 5 times, we report the maximum runtime.

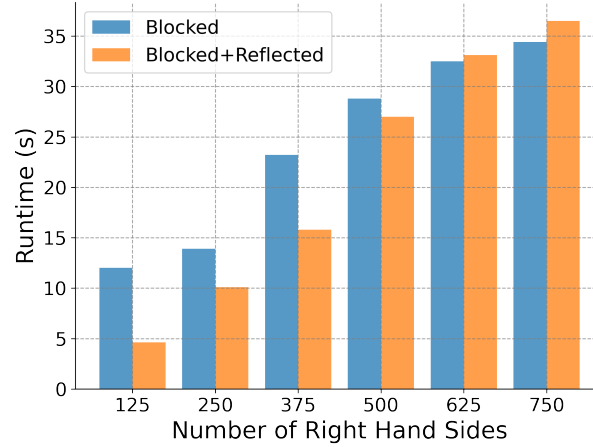


Figure 3.12: In this experiment we compared the runtime for blocking together matrix-matrix products corresponding to T^{M2L} for each of 316 transfer vectors (labelled ‘Blocked’), to blocking together matrix-matrix products for each of a reduced set of just 16 unique transfer vectors (labelled ‘Blocked + Reflected’). The left matrix is a random dense matrix generated using double precision floating point numbers, with dimensions matching T^{M2L} for expansion orders of 9, the right matrix is again a random dense matrix generated using double precision floating point numbers chosen to represent the multipole coefficients being translated. To estimate the runtime of application of the blocking approaches, we simply compute the matrix-matrix product with 20 times as many right hand sides ($316/16 = 19.75 \approx 20$) for the reduced blocking scheme, as the blocking scheme doesn’t reduce the number of flops in this approach. The matrix-matrix product for the naively blocked scheme is correspondingly computed repeatedly in a loop of length 20, ensuring that both approaches have a matching number of flops. We find that for smaller numbers of right-hand sides, the reducing the set of transfer vectors to make more efficient use of BLAS3 matrix-matrix products does help significantly, however for larger numbers of right-hand sides greater than approximately 500, which is typical for the FMM, there is little difference with this optimisation. Experiments are taken on a 6 core Intel i7-9750 processor using Open BLAS, we report maximum runtimes over 5 runs for each set of parameters.

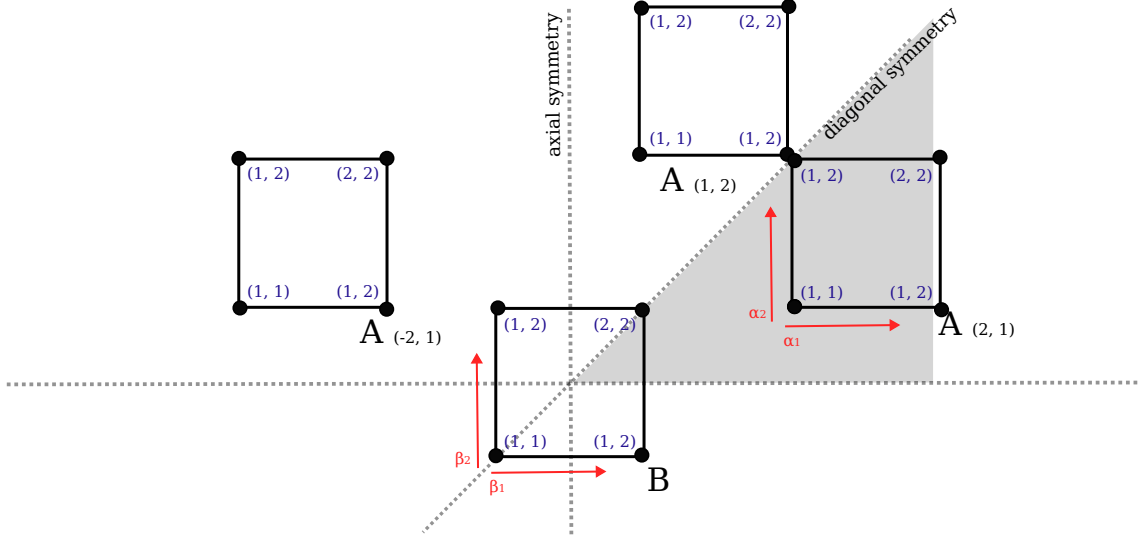


Figure 3.13: Here we show the axial and diagonal symmetries of three source boxes labelled A with respect to a target box B in \mathbb{R}^2 for expansion order $P = 2$. The quadrature points are labelled with index coordinates taken with respect to the lower left corner of the box. The only transfer vector here the constraints of being in the ‘reference cone’, which is shaded in grey, is $t = (2, 1)$ and therefore corresponds to the only T^{M2L} that needs to be pre-computed. This figure is adapted from [28] for the kiFMM as opposed to the bbFMM as originally presented.

$t_1 = 0$, $t_2 = 0$ and $t_3 = 0$ in \mathbb{R}^3 , each dividing \mathbb{R}^3 into two parts centered on the target box B . Combining all three plane divides \mathbb{R}^3 into octants centered on B , we refer to \mathbb{R}_+^3 as the *reference octant*. The diagonal planes of symmetry are given by $t_1 = t_2$, $t_1 = t_3$ and $t_2 = t_3$ in \mathbb{R}^3 . We restrict ourselves to diagonal symmetries that lie in the reference octant. Combining the axial and diagonal symmetries we obtain a *reference cone*,

$$\mathbb{R}_{\text{sym}}^3 = \{\mathbb{R}_{\text{sym}}^3 \subset \mathbb{R}^3 : t_1 \geq t_2 \geq t_3 \text{ with } t \in \mathbb{R}^3\} \quad (3.27)$$

We identify a subset of transfer vectors $T_{\text{sym}} = T \cap \mathbb{R}_{\text{sym}}^3$ from which all transfer vectors for B can be expressed as reflections around the axes of symmetry. Explicitly to find t within T_{sym} , we apply the following rule

1. A *axial symmetry* given by say $t_1 = 0$ as shown in Figure 3.13, we invert the corresponding component of the index coordinate

$$\alpha \leftarrow (P - (\alpha_1 - 1), \alpha_2, \alpha_3) \text{ and } \beta \leftarrow (P - (\beta_1 - 1), \beta_2, \beta_3)$$

2. A *diagonal symmetry* given by say $t_1 = t_2$, we swap the corresponding components of the index coordinate as,

$$\alpha \leftarrow (\alpha_2, \alpha_1, \alpha_3) \text{ and } \beta \leftarrow (\beta_2, \beta_1, \beta_3)$$

Where as before P stands for expansion order. When these rules are applied to the 316 unique transfer vectors for our kernels of interest, we find that $|T_{\text{sym}}| = 16$.

Utilising this redundancy for the FFT accelerated T^{M2L} means that one only has to precompute Fourier transform of Kernel sequences $K[\cdot]$ corresponding to transfer

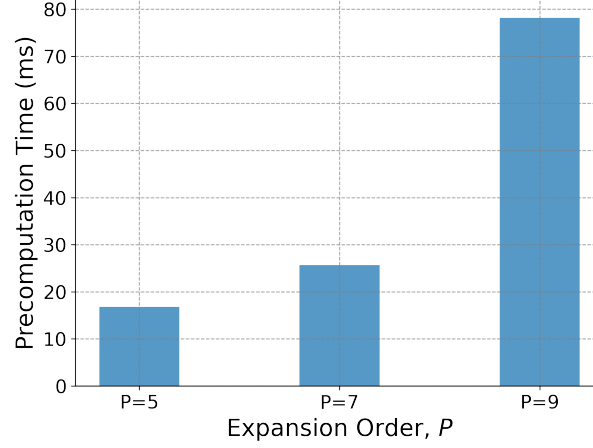


Figure 3.14: Here we illustrate the precomputation time to compute the FFTs required of T^{M2L} for a selection of expansion orders for all 316 unique transfer vectors for the Laplace kernel. We highlight the approximately 500x runtime advantage over the precomputations required for the SVD implementation (fig. 3.7). Experiments are taken on a 6 core Intel i7-9750 processor using Open BLAS, we report maximum runtimes over 5 runs for each set of parameters.

vectors in T_{sym} . In order to reduce the number of flops required for computing T^{M2L} during the algorithm we notice that T^{M2L} is calculated for a box B from a halo consisting of its interaction list, i.e. the children of B 's parent which it does not lie adjacent to. There is a conjugacy in this relationship meaning that if A is in that set of boxes for B , then B is correspondingly in that set of boxes for A . This means that we can ‘invert’ the application of the T^{M2L} operator. Instead of attempting to compute the check potential at B from boxes A in its halo, we can instead compute the convolutions corresponding to just 16 unique T^{M2L} for the multipole coefficients at B and scatter the resulting check potential to their corresponding boxes in B 's halo. This means that we are only computing 16 convolution operations with respect to each box, in comparison the 1664 as in previous implementations.

This transforms the problem into one that is bound by memory accesses. To alleviate this we take a similar approach to the state of the art softwares mentioned above, and consider sibling sets S at a time. We iterate over sibling sets in parallel, pulling in references to S 's parent's neighbours' children into memory in each parallel thread. These constitute all the scatter locations for the check potentials computed for each box in S . By doing this however we reduce the number of cache-misses during the scatter operation as we can save all the corresponding check potentials to a box in S 's halo at once. For the same benchmark problem above we reported for the state of the art approach of [25], we compute T^{M2L} in 6.8s⁷.

The effect of memory ordering and access on runtimes is clear, and significant, for this operation. As of writing we are still working on an optimal memory ordering in the implementation of this approach, which if we are able to find would constitute a new algorithm for sparsifying T^{M2L} via the FFT for algebraic FMMs discretised on regular grids, as the number flops in our approach is greatly reduced.

⁷Experiments were repeated 5 times, we report the maximum runtime.

Conclusion

In this subsidiary thesis we've presented progress on the development of a new software infrastructure for fast algorithms. We've documented recent outputs towards this goal including foundational software as well as algorithmic techniques. The main outputs being an investigation into programming languages and environments most suitable for scientific computing, investigations to ensure an ergonomic design for our software, a distributed load balanced octree library designed for high-performance, as well as significant inroads to a distributed FMM based on this by studying sparsification schemes for the multipole-to-local translation operator T^{M2L} .

The immediate next steps of this project will be to publish our recent software results on octrees and the parallel FMM in an appropriate scientific journal, and release a first version of our software. The final stages of this project will focus on completing the outlined improvements to our translation operator library to achieve, and hopefully supersede the current state of the art, creating a new benchmark distributed FMM library that is open to extension to other fast algorithms.

Deriving Local Expansion Coefficients from the Analytical Multipole Expansion in \mathbb{R}^2 for the Laplace kernel

Working in the setting in which we derived the multipole expansion in equation (2.9),

$$\phi(x) = \sum_{j \in I_s} K(x, y) q_j = \log(x - c_s) \hat{q}_0^s + \sum_{p=1}^{\infty} \frac{1}{(x - c_s)^p} \hat{q}_p^s \quad (\text{A.1})$$

Deriving the local expansion centered around the origin, where the bounding box of the targets, Ω_t , is well separated from the source box, Ω_s ,

$$\phi(x) = \sum_{l=0}^{\infty} \hat{\phi}_l^t (x - c_t)^l$$

from the multipole expansion relies on the following expressions,

$$\begin{aligned} \log((x - c_t) - c_s) &= \log(-c_s(1 - \frac{x - c_t}{c_s})) \\ &= \log(-c_s) - \sum_{l=1}^{\infty} \frac{1}{l} \left(\frac{x - c_t}{c_s} \right)^l \end{aligned}$$

and,

$$\begin{aligned} ((x - c_t) - c_s)^{-p} &= \left(\frac{-1}{c_s} \right)^p \left(\frac{1}{1 - \frac{x - c_t}{c_s}} \right)^p \\ &= \left(\frac{-1}{c_s} \right)^p \sum_{l=0}^{\infty} \binom{l + p - 1}{p - 1} \left(\frac{x - c_t}{c_s} \right)^l \end{aligned}$$

Substituting these expressions into (A.1), translated to be centred on Ω_t

$$\begin{aligned} \phi(x) &= \log((x - c_t) - c_s) \hat{q}_0^s + \sum_{p=1}^{\infty} \frac{1}{((x - c_t) - c_s)^p} \hat{q}_p^s \\ &= \log(-c_s) \hat{q}_0^s - \left(\sum_{l=1}^{\infty} \frac{1}{l} \left(\frac{x - c_t}{c_s} \right)^l \right) \hat{q}_0^s + \sum_{p=1}^{\infty} \left(\frac{-1}{c_s} \right)^p \sum_{l=0}^{\infty} \binom{l + p - 1}{p - 1} \left(\frac{x - c_t}{c_s} \right)^l \hat{q}_p^s \end{aligned}$$

Identifying the local expansion coefficients as,

$$\hat{\phi}_0^t = \hat{q}_0^s \log(-c_s) + \sum_{p=1}^{\infty} \frac{\hat{q}_p^s}{c_s^p} (-1)^p$$

and,

$$\hat{\phi}_l^t = \frac{-\hat{q}_0^s}{l c_s^l} + \frac{1}{c_s^l} \sum_{p=1}^{\infty} \frac{\hat{q}_p^s}{c_s^p} \binom{l+p-1}{p-1} (-1)^p$$

Hyksort

The parallel splitter selection and HykSort algorithms are provided below. In terms of complexity analysis, we adapt the analysis provided in section 3.4 of [36]. The main costs of SampleSort is sorting the splitters and the MPI collectives for data reshuffling. This can lead to a load imbalance and network congestion, represented by a constant c below,

$$T_{ss} = t_c c \frac{N}{p} \log \frac{N}{p} + (t_s + t_w o) \log^2 p + t_w c \frac{N}{p}$$

Where t_c is the intranode memory slowness (1/RAM bandwidth), t_s interconnect latency, t_w is the interconnect slowness (1/bandwidth), p is the number of MPI tasks in *comm*, and N is the total number of keys in an input array A , of length N .

The parallel splitter selection algorithm for determining k splitters uses MPI collectives, `All_Gather()` and `All_Reduce()`. The main cost is in determining the local ranks of the samples using a binary search. The number of iterations η depends on the input distribution, the required tolerance N_ϵ/N and the parameter β . The expected value of η varies as $\log(\epsilon)/\log(\beta)$ and β is chosen experimentally to minimise the running time, leading to a complexity of,

$$T_{ps} = \eta t_c \beta k \log \frac{N}{p} + \eta (t_s + t_w \beta k) \log p$$

HykSort relies on a specialised `All_to_all_kway()` collective, we defer to the original paper for details. It uses only point to point communications with staged message sends and receives, allowing HykSort to minimise network congestion. It has $\log p / \log k$ stages with $O(N/p)$ data transfer and k messages for each task in every stage. This leads to a complexity of,

$$T_{a2a} = \left(t_s k + t_w \frac{N}{p} \right) \frac{\log p}{\log k}$$

Finally, HykSort has the same communication pattern as `All_to_all_kway()`. In addition it relies on the parallel splitter selection algorithm to determine splitters. The main computational cost is the initial local sort, and merging k arrays during each iteration.

$$T_{Hk} = t_c \frac{N}{p} \log \frac{N}{p} + \left(t_c \frac{N}{p} + T_{ps} \right) \frac{\log p}{\log k} + T_{a2a} \quad (\text{B.1})$$

Unlike SampleSort, the complexity of HykSort doesn't involve any $O(p)$ terms. This is the term that can lead to network congestion for higher core counts.

Algorithm 1 Parallel Select

Input: A_r - array to be sorted (local to each process), n - number of elements in A_r , N - total number of elements, $R[0, \dots, k-1]$ - expected global ranks, N_ϵ - global rank tolerance, $\beta \in [20, 40]$,

Output: $S \subset A$ - global splitters, where A is the global array to be sorted, with approximate global ranks $R[0, \dots, k-1]$

$R^{\text{start}} \leftarrow [0, \dots, 0]$ - Start range of sampling splitters

$R^{\text{end}} \leftarrow [n, \dots, n]$ - End range of sampling splitters

$n_s \leftarrow [\beta/p, \dots, \beta/p]$ - Number of local samples, each splitters

$N_{\text{err}} \leftarrow N_\epsilon + 1$

while $N_{\text{err}} > N_\epsilon$ **do**

$Q' \leftarrow A_r[\text{rand}(n_s, (R^{\text{start}}, R^{\text{end}}))]$

$Q \leftarrow \text{Sort}(\text{All_Gather}(\hat{Q}'))$

$R^{\text{loc}} \leftarrow \text{Rank}(Q, A_r)$

$R^{\text{glb}} \leftarrow \text{All_Reduce}(R^{\text{loc}})$

$I[i] \leftarrow \text{argmin}_j |R^{\text{glb}} - R[I]|$

$N_{\text{err}} \leftarrow \max |R^{\text{glb}} - RI|$

$R^{\text{start}} \leftarrow R^{\text{loc}}[I-1]$

$R^{\text{end}} \leftarrow R^{\text{loc}}[I+1]$

$n_s \leftarrow \beta \frac{R^{\text{end}} - R^{\text{start}}}{R^{\text{glb}}[I+1] - R^{\text{glb}}[I-1]}$

end while

return $S \leftarrow Q[I]$

Algorithm 2 HykSort

Input: A_r - array to be sorted (local to each process), $comm$ - MPI communicator, p - number of processes, p_r - rank of current task in $comm$

Output: globally sorted array B .

while $p > 1$, Iters: $O(\log p / \log k)$ **do**

$N \leftarrow \text{MPI_AllReduce}(|B|, comm)$

$s \leftarrow \text{ParallelSelect}(B, \{iN/k; i = 1, \dots, k-1\})$

$d_{i+1} \leftarrow \text{Rank}(s_i, B), \forall i$

$[d_0, d_k] \leftarrow [0, n]$

$color \leftarrow \lfloor kp_r/p \rfloor$

parfor $i \in 0, \dots, k-1$ **do**

$p_{recv} \leftarrow m((color - i) \bmod k) + (p_r \bmod m)$

$R_i \leftarrow \text{MPI_Irecv}(p_{recv}, comm)$

end parfor

for $i \in 0, \dots, k-1$ **do**

$p_{recv} \leftarrow m((color - i) \bmod k) + p_r \bmod m$

$p_{send} \leftarrow m((color + i) \bmod k) + p_r \bmod m$

$j \leftarrow 2$

while $i > 0$ and $i \bmod j = 0$ **do**

$R_{i-j} \leftarrow \text{merge}(R_{i-j}, R_{i-j/2})$

$j \leftarrow 2j$

end while

$\text{MPI_WaitRecv}(p_{recv})$

end for

$\text{MPI_WaitAll}()$

$B \leftarrow \text{merge}(R_0, R_{k/2})$

$comm \leftarrow \text{MPI_Comm_splitt}(color, comm)$

$p_r \leftarrow \text{MPI_Comm_rank}(comm)$

end while

return B

The Adaptive Fast Multipole Method Algorithm

FMM literature distinguishes between types of relationships between neighbouring nodes with the concept of *interaction lists*. There are four such lists for a given node B , called V , U , W and X . For a leaf node B , the U list contains B itself and leaf nodes adjacent to B . and the W list consists of the descendants of B 's neighbours whose parents are adjacent to B . For non-leaf nodes, the V list is the set of children of the neighbours of the parent of B which are not adjacent to B , and the X list consists of all nodes A such that B is in their W lists. The non-adaptive algorithm is similar, however the W and X lists are empty

Algorithm 3 Adaptive Fast Multipole Method.

N is the total number of points

s is the maximum number of points in a leaf node.

Step 1: Tree construction

for each node B in *preorder* traversal of tree, i.e. the nodes are traversed bottom-up, level-by-level, beginning with the finest nodes. **do**

 subdivide B if it contains more than s points.

end for

for each node B in *preorder* traversal of tree **do**

 construct *interaction lists*, U , V , X , W

end for

Step 2: Upward Pass

for each leaf node B in *postorder* traversal of the tree, i.e. the nodes are traversed top-down, level-by-level, beginning with the coarsest nodes. **do**

P2M: compute multipole expansion for the particles they contain.

end for

for each non leaf node B in *postorder* traversal of the tree **do**

M2M: form a multipole expansion by translating the expansion centre of its children to its centre and summing their multipole expansion coefficients.

end for

Step 3: Downward Pass

for each non-root node B in *preorder* traversal of the tree **do**

M2L: translate multipole expansions of nodes in B 's V list to a local expansion at B .

P2L: translate the charges of particles in B 's X to the local expansion at B .

L2L: translate B 's local expansion to its children by translating its expansion centre to the centre of its children, and assigning the same coefficients.

end for

for each leaf node B in *preorder* traversal of the tree **do**

P2P: directly compute the local interactions using the kernel between the particles in B and its U list.

L2P: translate local expansions for nodes in B 's W list to the particles in B .

M2P: translate the multipole expansions for nodes in B 's W list to the particles in B .

end for

Well Posedness of Dirichlet Boundary Value Problems For The Laplace Equation

Consider the Laplace equation,

$$\Delta\phi = 0 \tag{D.1}$$

Solutions of which are described as ‘harmonic’. The fundamental solutions, or kernel, (2.2) are harmonic in $\mathbb{R}^n \setminus \{y\}$. To formulate a boundary value problem for the Laplace equation, consider a bounded domain $\Omega_- \in \mathbb{R}^n$ which supports C^2 functions, with a boundary $\partial\Omega_-$, its open complement $\Omega_+ := \mathbb{R}^n \setminus \bar{\Omega}_-$, as well as a unit normal n pointing outwards into its exterior Ω_+ . We can define two prototypical boundary value problems based on a Dirichlet boundary condition,

Definition D.0.1 (Exterior Dirichlet Problem) *Find a function $\phi \in C^2(\Omega_+) \cap C(\bar{\Omega}_-)$ which is harmonic over Ω_+ and satisfies,*

$$\phi = f, \text{ on } \partial\Omega_-$$

where f is a given continuous function. For $|x| \rightarrow \infty$ it's required that,

$$\phi(x) = O(1)$$

if $m = 2$, and

$$\phi(x) = o(1)$$

if $m = 3$, uniformly in all directions $x/|x|$

Definition D.0.2 (Interior Dirichlet Problem) *Find a function $u \in C^2(\Omega_-) \cap C(\bar{\Omega}_-)$ which is harmonic over Ω_- and satisfies,*

$$\phi = f, \text{ on } \partial\Omega_-$$

where f is a given continuous function.

Problems of this form appear with great frequency in Physics and Engineering. They appear in electrostatics, heat flow, and fluid flow and many many more fields. We want to establish well-posedness, i.e. uniqueness, in the solution of each of these problems.

Theorem D.0.1 (Dirichlet Problems) *The interior and exterior Dirichlet problems are unique.*

Proof:

Let ϕ_1 and ϕ_2 be two harmonic functions in some region Ω , satisfying the Dirichlet boundary condition on $\partial\Omega$. Then $\phi := \phi_1 - \phi_2$ is also harmonic with $\phi = 0$ Dirichlet boundary conditions. Using the minimum-maximum principle we see that $\phi \equiv 0$ in Ω . As ϕ is of $O(1)$ (or $o(1)$, depending on dimension) in the exterior uniformly in all directions, we see that $\phi \equiv 0$ in the exterior too. Thus proving our claim.

Distributed Octrees

E.1 Useful Properties of Morton Encodings

These properties are taken from Appendix A in [37]

1. Sorting the leaves by their Morton keys is equivalent to pre-order traversal of an octree. If one connects the centers of the boxes in this order we observe a ‘Z’-pattern in Cartesian space. Nearby octants in Morton order are clustered together in Cartesian space.
2. Given three octants $a < b < c$ and $c \notin \text{Descendants}(b)$

$$a < d < c \forall d \in \{\text{Descendants}(b)\}$$

3. The Morton key of any box is less than those of its descendants.
4. Two distinct octants overlap only if and only if one is an ancestor of another.
5. The Morton key of any node and its first child are consecutive.
6. The first descendant at level l , $\text{FirstDescendant}(N, l)$ of any box N is the descendant at that level with the least Morton key.
7. The range $(N, \text{DeepestFirstDescendant}(N)]$ contains only the first descendants of N at different levels, and hence there can be no more than one leaf in this range in the entire linear octree.
8. The last descendant at level l of N , $\text{LastDescendant}(N, l)$ of any node N is the descendant at that level with the greatest Morton key.
9. Every octant in the range $(N, \text{DeepestLastDescendant}(N)]$ is a descendant of N .

E.2 Algorithms Required for Constructing Distributed Linear Octrees

These listings are adapted from [37].

Algorithm 4 Remove Overlaps From Sorted List of Octants (Sequential) - Linearise. Favour smaller octants over larger overlapping octants.

Input: A sorted list of octants, W .
Output: R , an octree with no overlaps.
Work: $O(n)$, where $n=\text{len}(W)$.
Storage: $O(n)$, where $n=\text{len}(W)$.
for $i \leftarrow 1$ **to** $\text{len}(W)$ **do**
 if $W[i] \notin \{\text{Ancestors}(W[i+1]), W[i+1]\}$ **then**
 $R \leftarrow R + W[i]$
 end if
end for
 $R \leftarrow R + W[\text{len}(i)]$

Algorithm 5 Construct a Minimal Linear Octree Between Two Octants (Sequential) - CompleteRegion.

Input: Two octants a and b , where $a > b$ in Morton order.
Output: R , minimal linear octree between a and b .
Work: $O(n \log n)$, where $n=\text{len}(R)$.
Storage: $O(n)$, where $n=\text{len}(R)$.
for $w \in W$ **do**
 if $a < w < b$ **and** $w \notin \{\text{Ancestors}(b)\}$ **then**
 $R \leftarrow R + w$
 else if $w \notin \{\text{Ancestors}(a), \text{Ancestors}(b)\}$ **then**
 $W \leftarrow W - w + \text{Children}(w)$
 end if
end for
Sort(R)

Algorithm 6 Balance a Local Octree (Sequential) - Balance. A 2:1 balancing is enforced, such that adjacent octants are at most twice as large as each other.

Input: A local octree W , on a given node.
Output: R , a 2:1 balanced octree.
Work: $O(n \log n)$, where $n=\text{len}(R)$.
Storage: $O(n)$, where $n=\text{len}(W)$.
 $R = \text{Linearize}(W)$
for $l \leftarrow \text{Depth}$ **to** 1 **do**
 $Q \leftarrow \{x \in W \mid \text{Level}(x) = l\}$
 for $q \in Q$ **do**
 for $n \in \{\text{Neighbours}(q), q\}$ **do**
 if $n \notin R$ **and** $\text{Parent}(n) \notin R$ **then**
 $R \leftarrow R + \text{Parent}(n)$
 $R \leftarrow R + \text{Siblings}(\text{Parent}(n))$
 end if
 end for
 end for
end for

Algorithm 7 Construct Distributed Octree (Parallel)

Input: A distributed list of points L , and a parameter n_{crit} specifying the maximum number of points per octant.
Output: A complete linear octree, B .
Work: $O(n \log n)$, where $n = \text{len}(L)$.
Storage: $O(n)$, where $n = \text{len}(L)$.
 $F \leftarrow [\text{Octant}(p, \text{MaxDepth}), \forall p \in L]$
ParallelSort(F)
 $B \leftarrow \text{BlockPartition}(F)$, using algorithm (8)
for $b \in B$ **do**
 if NumberOfPoints(b) $> n_{\text{crit}}$ **then**
 $B \leftarrow B - b + \text{Children}(b)$
 end if
end for

Optional Balancing over subtrees, f .
if Balance = True **then**
 for $f \in F$ **do**
 Balance(f), using algorithm (6)
 end for
ParallelSort(F)
 for $f \in F$ **do**
 Linearise(f), using algorithm (4)
 end for
end if

Algorithm 8 Partitioning Octants Into Coarse Parallel Blocks (Parallel) - BlockPartition.

Input: A distributed list of octants F .
Output: A list of blocks G , F redistributed but the relative order of the octants is preserved.
Work: $O(n)$, where $n = \text{len}(F)$.
Storage: $O(n)$, where $n = \text{len}(F)$.
 $T \leftarrow \text{CompleteRegion}(F[1], F[\text{len}(F)])$, using algorithm (5)
 $C \leftarrow \{x \in T \mid \forall y \in T, \text{Level}(x) \leq \text{Level}(y)\}$
 $G \leftarrow \text{CompleteOctree}(C)$, using algorithm (9)
for $g \in G$ **do** weight(g) $\leftarrow \text{len}(F_{\text{global}} \cap \{g, \{\text{Descendants}(g)\}\})$
end for
 $F \leftarrow F_{\text{global}} \cap \{g, \{\text{Descendants}(g)\} \mid g \in G\}$

Algorithm 9 Construct a Complete Linear Octree From a Set of Seed Octants Spread Across Processors (Parallel) - CompleteOctree

Input: A distributed sorted list of seeds L .
Output: R , a complete linear octree.
Work: $O(n \log n)$, where $n = \text{len}(R)$.
Storage: $O(n)$, where $n = \text{len}(R)$.
 $L \leftarrow \text{Linearise}(L)$, using algorithm (4).
if rank = 0 **then**
 $L.\text{push_front}(\text{FirstChild}(\text{FinestAncestors}(\text{DeepestFirstDescendent}(\text{root}), L[1])))$
end if
if rank = $n_p - 1$ **then**
 $L.\text{push_back}(\text{LastChild}(\text{FinestAncestors}(\text{DeepestLastDescendent}(\text{root}), L[\text{len}(L)])))$
end if
if rank \neq 0 **then**
 Send($L[1]$, (rank-1))
end if
if rank \neq ($n_p - 1$) **then**
 $L.\text{push_back}(\text{Receive}())$
end if
for $i \leftarrow 1$ to ($\text{len}(L)-1$) **do**
 $A \leftarrow \text{CompleteRegion}(L[i], L[i + 1])$, using algorithm (5)
end for
if rank = $n_p - 1$ **then**
 $R \leftarrow R + L[L]$
end if

Bibliography

- [1] Sivaram Ambikasaran and Eric Darve. “The inverse fast multipole method”. In: *arXiv preprint arXiv:1407.1572* (2014).
- [2] *B2: makes it easy to build C++ projects, everywhere*. 2022. URL: <https://github.com/boostorg/build>.
- [3] *Bazel - a fast, scalable, multi-language and extensible build system*. Version 5.3.2. 2022. URL: <https://github.com/bazelbuild/bazel>.
- [4] Jeff Bezanson et al. “Julia: A fresh approach to numerical computing”. In: *SIAM review* 59.1 (2017), pp. 65–98.
- [5] *BLAS and LAPACK for Rust*. 2022. URL: <https://github.com/blas-lapack-rs>.
- [6] Steffen Boerm et al. *H2Lib: A software for hierarchical and H2 matrices*. Version 3.0.0. URL: <https://github.com/H2Lib/H2Lib>.
- [7] Steffen Börm, Lars Grasedyck, and Wolfgang Hackbusch. “Introduction to hierarchical matrices with applications”. In: *Engineering analysis with boundary elements* 27.5 (2003), pp. 405–422.
- [8] Carsten Burstedde, Lucas C. Wilcox, and Omar Ghattas. “p4est: Scalable Algorithms for Parallel Adaptive Mesh Refinement on Forests of Octrees”. In: *SIAM Journal on Scientific Computing* 33.3 (2011), pp. 1103–1133. DOI: 10.1137/100791634.
- [9] Shiv Chandrasekaran et al. “A fast solver for HSS representations via sparse matrices”. In: *SIAM Journal on Matrix Analysis and Applications* 29.1 (2007), pp. 67–81.
- [10] Barry A Cipra. “The best of the 20th century: Editors name top 10 algorithms”. In: *SIAM news* 33.4 (2000), pp. 1–2.
- [11] *Conan - The open-source C/C++ package manager*. Version 1.53.0. 2022. URL: <https://github.com/conan-io/conan>.
- [12] William Fong and Eric Darve. “The black-box fast multipole method”. In: *Journal of Computational Physics* 228.23 (2009), pp. 8712–8725.
- [13] *Fortran Package Manager (fpm)*. Version 0.7.0. 2022. URL: <https://github.com/fortran-lang/fpm>.
- [14] Leslie Greengard and Vladimir Rokhlin. “A fast algorithm for particle simulations”. In: *Journal of computational physics* 73.2 (1987), pp. 325–348.
- [15] Wolfgang Hackbusch. “A sparse matrix arithmetic based on H-matrices. part i: Introduction to H-matrices”. In: *Computing* 62.2 (1999), pp. 89–108.

- [16] Nathan Halko, Per-Gunnar Martinsson, and Joel A Tropp. “Finding structure with randomness: Probabilistic algorithms for constructing approximate matrix decompositions”. In: *SIAM review* 53.2 (2011), pp. 217–288.
- [17] Wilhelm Hasselbring et al. “Open source research software”. In: *Computer* 53.8 (2020), pp. 84–88.
- [18] Huda Ibeid, Rio Yokota, and David Keyes. “A performance model for the communication in fast multipole methods on high-performance computing platforms”. In: *International Journal of High Performance Computing Applications* 30.4 (2016), pp. 423–437. ISSN: 17412846. DOI: 10.1177/1094342016634819. arXiv: arXiv:1405.6362v1.
- [19] Srinath Kailasa et al. “PyExaFMM: an exercise in designing high-performance software with Python and Numba”. In: *Computing in Science & Engineering* 24.5 (2022), pp. 77–84.
- [20] Rainer Kress. *Linear integral equations*. Vol. 82. 2014, pp. i–412. ISBN: 9781461495925. DOI: 10.1007/978-1-4614-9593-2.
- [21] Siu Kwan Lam, Antoine Pitrou, and Stanley Seibert. “Numba: A llvm-based python jit compiler”. In: *Proceedings of the Second Workshop on the LLVM Compiler Infrastructure in HPC*. 2015, pp. 1–6.
- [22] Ilya Lashuk et al. “A massively parallel adaptive fast multipole method on heterogeneous architectures”. In: *Communications of the ACM* 55.5 (2012), pp. 101–109. ISSN: 0001-0782. DOI: 10.1145/2160718.2160740. URL: <https://dl.acm.org/doi/10.1145/2160718.2160740>.
- [23] Chris Lattner. *Mojo - a new programming language for all AI developers*. <https://www.modular.com/mojo>. 2023.
- [24] Denis Zorin Lexing Ying George Biros. “A kernel-independent adaptive fast multipole algorithm in two and three dimensions”. In: *Journal of Computational Physics* 196.2 (2004), pp. 591–626. DOI: <http://dx.doi.org/10.1016/j.jcp.2003.11.021>.
- [25] Dhairya Malhotra and George Biros. “PVFMM: A parallel kernel independent FMM for particle and volume potentials”. In: *Communications in Computational Physics* 18.3 (2015), pp. 808–830.
- [26] *Maturin*. Version 0.13.0. 2022. URL: <https://github.com/Py03/maturin>.
- [27] Matthias Messner, Martin Schanz, and Eric Darve. “Fast directional multi-level summation for oscillatory kernels based on Chebyshev interpolation”. In: *Journal of Computational Physics* 231.4 (2012), pp. 1175–1196.
- [28] Matthias Messner et al. “Optimized M2L kernels for the Chebyshev interpolation based fast multipole method”. In: *arXiv preprint arXiv:1210.7292* (2012).
- [29] *ndarray: an N-dimensional array with array views, multidimensional slicing, and efficient operations*. Version 0.15.6. 2022. URL: <https://github.com/rust-ndarray/ndarray>.
- [30] Rahul S Sampath et al. “Dendro: parallel algorithms for multigrid and AMR methods on 2: 1 balanced octrees”. In: *SC’08: Proceedings of the 2008 ACM/IEEE Conference on Supercomputing*. IEEE. 2008, pp. 1–12.
- [31] *SCons - a software construction tool*. Version 4.4.0. 2022. URL: <https://github.com/SCons/scons>.

- [32] Craig Scott. *Professional CMake: A Practical Guide*. 2018.
- [33] *Spack - A flexible package manager that supports multiple versions, configurations, platforms, and compilers*. Version 0.18.1. 2022. URL: <https://github.com/spack/spack>.
- [34] Benedikt Steinbusch and Andrew Gaspar et al. *RSMPi: MPI bindings for Rust*. Version 0.5.4. 2018. URL: <https://github.com/rsmpi/rsmpi>.
- [35] Josh Stone and Niko Matsakis et. al. *Rayon: A data parallelism library for Rust*. Version 1.5.3. 2022. URL: <https://github.com/rayon-rs/rayon>.
- [36] Hari Sundar, Dhairya Malhotra, and George Biros. “Hyksort: a new variant of hypercube quicksort on distributed memory architectures”. In: *Proceedings of the 27th international ACM conference on international conference on supercomputing*. 2013, pp. 293–302.
- [37] Hari Sundar, Rahul S Sampath, and George Biros. “Bottom-up construction and 2: 1 balance refinement of linear octrees in parallel”. In: *SIAM Journal on Scientific Computing* 30.5 (2008), pp. 2675–2708.
- [38] *The Meson Build System*. Version 0.63.3. 2022. URL: <https://github.com/mesonbuild/meson>.
- [39] Lloyd Nicholas Trefethen and David III Bau. *Numerical Linear Algebra*. Philadelphia: Society for Industrial and Applied Mathematics, 1997. ISBN: 0898713617.
- [40] Tiankai Tu, David R O’Hallaron, and Omar Ghattas. “Scalable parallel octree meshing for terascale applications”. In: *SC’05: Proceedings of the 2005 ACM/IEEE conference on Supercomputing*. IEEE. 2005, pp. 4–4.
- [41] *VCPKG - C++ Library Manager for Windows, Linux, and MacOS*. Version 2022.10.19. 2022. URL: <https://github.com/microsoft/vcpkg>.
- [42] Bruce Wagar. “Hyperquicksort: A fast sorting algorithm for hypercubes”. In: *Hypercube Multiprocessors* 1987 (1987), pp. 292–299.
- [43] Tingyu Wang, Rio Yokota, and Lorena A Barba. “ExaFMM: a high-performance fast multipole method library with C++ and Python interfaces”. In: *Journal of Open Source Software* 6.61 (2021), p. 3145.
- [44] Rio Yokota, George Turkiyyah, and David Keyes. “Communication complexity of the fast multipole method and its algebraic variants”. In: *Supercomputing Frontiers and Innovations* 1.1 (2014), pp. 62–83. ISSN: 23138734. DOI: 10.14529/jsfi140104. arXiv: 1406.1974.